CHAPTER IV

BLENDS OF CARBOXYLATE ACID POLYMER BASED ON HIGH-DENSITY POLYETHYLENE WITH NYLON: EFFECT OF ZINC NEUTRALIZED VERSUS ACID FORM HDPE-G-MAH

4.1 ABSTRACT

Ternary blends of PA6/HDPE/HDPE-g-MAH(Fusabond®) were prepared by melt mixing in a twin screw extruder. ZnO was introduced to the polymer blend system and expected to improve the efficiency of the compatibilizer (HDPE-g-MAH, Fusabond®). The phase morphology, mechanical properties and thermal behavior of these blends were investigated over a range of compositions. The addition of compatibilizer resulted in improved mechanical properties as compared with the uncompatibilized blends. SEM micrographs show that the addition of small amount of compatibilizer improved the compatibility of PA6/HDPE blends as evidenced by a reduction indispersed size from 14 μm to 3.8 μm; this reduction was achieved at a compatibilizer level of 1.0 wt%. The enhancement of the compatibility of PA6 and HDPE by addition of compatibilizer was also confirmed through thermal analysis. The decreased in the crystallization temperatures on addition of compatibilizer suggested that there are interactions between PA6 and HDPE-g-MAH occurred in the blend and this retarded the crystallization of the blend component. However, the blends that added ZnO were not observed in terms of phase morphology, thermal behavior and mechanical properties. Moreover, the shifting of loss modulus peaks in DMA results of blends containing compatibilizer indicated that there are some improvements in the compatibility of resulting blends including ZnO blending system. During blending, chemical and/or physical reactions had taken place between PA6, HDPE-g-MAH and ZnO.

Keywords: Polyamide 6, High-density polyethylene, Compatibilizer, Polymer blend, Phase morphology, Mechanical properties, Thermal behavior

4.2 INTRODUCTION

Blending of polymers is an excellent way for developing new materials with improved properties, although most blends are immiscible. Immiscible blend morphology generally can either be co-continuous if the two blend components have roughly equal volume fractions, or the minor component can form discrete domains inside the major component continuous phase. The size and shape of the domains greatly depend upon several factors, such as the ratio of the melt viscosity of components, interfacial tension and adhesion, and processing parameters. The properties of such mixtures depend on the properties of two polymers and the interfacial characteristics. If two incompatible polymers are blended, for example polar polyamide and non-polar polyethylene, the interfacial adhesion is poor and the blend has poor mechanical properties. Unfavorable interactions lead to large phase sizes and poor interfacial adhesion, which are the primary causes for the inferior mechanical properties. Effective compatibilization is the key to successful commercialization of immiscible polymer blends. One approach is to use macromolecules such as graft or block copolymers that act as interfacial agents. Another approach is reactive compatibilization; in recent years, reactive compatibilization of polymer blends has been the subject of much interest.

Knowledge of how the blend components interact is necessary in order to have an idea of the expected properties. Much work has been reported on blends of nylon with rubbers and polyolefin. The reported work has been dedicated to the study of nylon 6 with polyolefin, such as high-density polyethylene (HDPE), low-density polyethylene (LDPE), ethylene propylene rubber, and ethylene-based propylene diene monomer. Compatibilization of these ethylene based polymers has been achieved through use of copolymer or adducts of maleic anhydride [1] different acrylates such as polyethylene-graft-butylacrylate [2] and polyethylene-methacrylic acid isobutyl acrylate terpolymer [3]. The observed change has been explained on the basis of possible interfacial reaction between amine groups in nylon 6 and the carboxylic groups in the copolymers.

The functionalization of polyethylene with a small amount of ionic group is a particular attractive way of compatibilizing polyamide with polyethylene because

the amide group may interact with the ionomer via hydrogen bonding, ion-dipole interactions, or/and metal ion coordination during melt blending [4,5]. The introduction of such specific interaction can improve compatibility and may promote miscibility of polyamide and polyethylene blends [6-10].

Nylon 6 is an important engineering thermoplastic having good melt flow, high heat resistance, high strength, high rigidity and good barrier properties. However, nylon 6 has poor dimensional stability, high water absorption and poor impact strength. Therefore, nylon can be blended with a polymer having a high impact strength; an example is the Surlyn® Reflection series where nylon is blended with a ethylene-methacrylic acid copolymer partially neutralized with zinc [7]. The purpose of this work is to investigate blends of nylon with another polymer, specifically high-density polyethylene (HDPE). HDPE is a polyolefin widely employed in the packaging and the injection-molding industries. HDPE forms good moisture barriers and possesses very good tensile and impact strength. Polyethylene and nylon 6 are not compatible and hence blending of these materials result in poor properties. We believe this compatibility can be improved by the addition of a compatibilizer.

In this study, blends of nylon 6 and high-density polyethylene (HDPE) using maleic anhydride grafting on high-density polyethylene (HDPE-g-MAH) as a compatibilizer were investigated. DuPont markets this compatibilizer under the trademark Fusabond®. Moreover HDPE-g-MAH can be partially neutralized with zinc, and the effects of this neutralization was studied. Attentions were focused on the thermal behavior, rheological properties, mechanical properties and phase morphology of these blends as a function of the compatibilizer content.

4.3 EXPERIMENTAL

Materials

Polyamide 6 employed in this study was an injection-molding grade (1013B), supplied by UBE nylon (Thailand). The HDPE was also an injection-molding grade (H5480S) supplied by Thai polyethylene Co., Ltd. The HDPE-g-

MAH under the trademark Fusabond® E MB 100D (0.9 wt% MAH graft level), was supplied by DuPont, USA. Finally, ZnO was obtained from Ajax Finechem.

Blends Preparation

Both uncompatibilized and compatibilized blends were prepared by a relatively similar procedure.

Pellets were mixed in a trumble mixer for 10 min. Followed by drying under vacuum at 60°C at least 12 hrs. The materials were blended in a Collin D-8017 T-20 twin screw extruder using a screw speed of 35 rpm; the processing conditions were the following temperature (°C): 75, 200, 215, 220, 220 and 230 from hopper to die, respectively. The blends were extruded through a single strand die; the extrudates were cooled in a water bath, dried at ambient temperature and then pelletized. The binary PA6/HDPE blends were prepared with weight ratios of 80/20 and 20/80. When a compatibilizer was employed, 0.1-10 parts of it were added to 100 parts of the blends. The pellets obtained were dried and kept in the sealed plastic bags prior to compression molding, so that the moisture regain of the blends would be minimize.

Specimen Preparation

Test specimens were prepared using a Wabash V 50 H 50 ton compression molding machine. Pellets were placed in a picture frame mold and the mold is preheated at 240°C for 3 minutes in the press without application of pressure. The mold was then compressed under a force of 10 tons for a further 3 minutes after which the mold is cooled to 40°C under pressure. Test specimens were cut from the molded sheets using a pneumatic die cutter.

Phase Morphology

Scanning electron microscope (SEM), JEOL 5200-2AE (MP152001) was used to study phase morphologies of the blends. The specimens were fractured in liquid nitrogen and etched using (i) hot decalin (for HDPE minor phase blends) and (ii) formic acid (for PA6 minor phase blends). The specimens were then coated with gold under vacuum. All SEM studied were characterized using magnification of

1500 times at 15-20 kV. The specimens were then coated with gold, under vacuum, to make them electrically conductive. The number average diameter (d_n) was calculated using equation (1)

$$d_n = \sum(n_i d_i)/(n_i) \quad (1)$$

where n_i is the number of droplet and d_i is the diameter of the *i*th droplet.

Differential Scanning Calorimetric Analysis

The thermal analysis was carried out on a differential scanning calorimeter, Perkin-Elmer DSC 7. All scans were made under nitrogen atmosphere to minimize oxidative degradation. The temperature calibration of DSC was obtained by measuring the melting temperature of indium. About 10 mg samples were exposed to the following conditions: the specimens, encapsulated in aluminum pans, were heated from 30°C to 250°C at a heating rate of 80°C/min, held for 5 minutes at this temperature to remove their thermal history, followed by cooling to 30°C at 10°C/min. The crystallinity of the sample was also determined from a knowledge of the ratio of the melting enthalpy for 100% crystallinity of pure components. The absolute crystallinity of the blend was calculated using equation (2),

$$\chi_c = \frac{\Delta H \times 100\%}{\Delta H_f \times \text{wt.fraction}} \quad (2)$$

where χ_c is the % weight fractional crystallinity, ΔH is the melting enthalpy of the component present in the blends, ΔH_f is the heat of fusion for the 100% crystallinity of the pure component, (190 J/g for Ny6, and 293 J/g for HDPE)

Mechanical and Physical Properties Testing

Tensile properties, impact property and hardness of the blends were determined from the compressed specimens following the test conditions suggested by ASTM.

An Instron Universal testing machine was used to measure the tensile strength of the blends. The tests were conducted according to ASTM D638-91 test procedure, using a crosshead speed of 50 $mm.mim^{-1}$. The tensile modulus, stress at break and elongation at break were determined from the curves. Izod impact strength was measured using a Zwick Impact tester according to ASTM D 256-92 test procedure method with a 2.7 J pendulum. Shore D hardness tester was used to measure hardness of the blends. The test was conducted according to, ASTM D 2240 test procedure.

All the tests were done at room temperature (30°C) and the results were obtained from the average of ten specimens for each blend ratio.

X-ray Diffraction Analysis

Wide angle X-ray diffraction (WAXS) investigation of the neat PA6 and HDPE as well as their blends were carrier out at room temperature using a Bruker AXS D8 Discover system with a 2-D wire detector. Samples were measured in symmetric transmission; two different source-detector angles were used and the data was combined by matching the intensities in the overlap region. Within experimental error, this procedure was identical to matching the two spectra by using the known angular correction for the two angles. No angular correction was performed for different sample absorption depending on angle for a given source-detector angle; the transmittance of all samples was fairly high (~80%) and no distortions were apparent in the overlap region. The transmittance was not used to subtract the background spectra from the sample spectra, rather the transmittance was set at a value that gave a flat profile at low angles.

Dynamic Mechanical Analysis

Dynamic mechanical of these blends were studied using a Solid Analyzer RSA II (Rheometric scientific). The storage modulus (E') and loss modulus (E") were measured as a function of temperature. The 3 point bend fixture was used to mount the samples and temperature step of 4 K intervals. All experiments were performed at 1 Hz frequency and 0.025% strain amplitude using static force tracing dynamic force.

4.4 RESULTS AND DISCUSSION

Phase morphology

All the blends were prepared by melt mixing of HDPE, PA6, HDPE-g-MAH (Fusabond®) and ZnO in a twin-screw extruder at 240°C and the extrudates were cooled by water. The morphology of different blends was investigated by scanning electron microscope (SEM) on freeze-fracture specimens. The SEM micrograph of fracture surfaces of uncompatibilized blends showed a clear-cut, two phase morphology with phase separation between PA6 and HDPE phases as shown in Figure 4.1. The presence of dispersed phase, consisting of predominantly spherical droplets imbedded in a matrix, was clearly observed from the micrographs of the whole composition range. It is obvious from Figure 4.1 that the adhesion between PA6 and HDPE was very poor, as expected. The micrographs of the compatibilized PA6/HDPE blends are shown in Figures 4.2 and 4.4. When the small amount of the compatibilizer was added. It resulted in decrease of the dispersed particle size for both HDPE and PA6 as a dispersed phase. The reduction of dispersed phase size when the compatibilizer was added, was due to the ability of the compatibilizer to reduce the interfacial tension between the dispersed phase and the matrix phase. The reduction of the interfacial tension could be caused by the chemical reaction between the terminal amine group in PA6 and the maleic anhydride functional group in the compatibilizer increased the interfacial adhesion of the blend. This interaction can be confirmed using the Molau test, by adding of formic acid to blends [2,11]. For uncompatibilied blend, a separation of PA6 from HDPE was observed, whereas the PA6/HDPE/Fusabond® blends gave rise to colloidal suspension in formic acid. The number average size of the particle diameter of dispersed phase of the compatibilized blends is reported in Figure 4.6. It was found that approximately 1.0 phr of Fusabond® was sufficient to produce a maximum reduction of dispersed phase size. The micrographs of the compatibilized PA6/HDPE blends added with ZnO are shown in Figures 4.3 and 4.5 are very similar to that of the no added ZnO.

Differential scanning calorimetry

Effect of compatibilizer on the melting and crystallization temperatures of each component of the blends were studied.

Figure 4.7 shows DSC exothermic thermograms of PA6/HDPE blends. The crystallization temperature (T_c) peak of pure PA6 and pure HDPE occurred at 178.5°C and 110.1°C, respectively. No change in T_c of the HDPE component in the PA/HDPE blends was observed. On the other hand, T_c of PA6 component is barely discernible higher than T_c of pure PA6. It is possible that the phase boundary interface between PA6 and HDPE phases behaves as a nucleation site for PA6. DSC exothermic thermograms of PA6/HDPE blends at various compatibilizer contents are shown in Figures 4.8 and 4.10. In PA6/HDPE 80/20 blends (Figure 4.8), the addition of compatibilizer resulting in no change in T_c of the HDPE component but T_c of PA6 component is barely discernible higher than T_c of pure PA6. In addition, for PA6/HDPE 20/80 blends (Figure 4.10), the effect of addition of compatibilizer on the T_c peak of PA6 and HDPE components is relatively similar to that of the PA6/HDPE 80/20 blends. However, at the compatibilizer rich blend (2.5-10%wt.), the T_c peak of PA6 component could not be observed. DSC exothermic thermograms of PA6/HDPE blends at various compatibilizer contents and added ZnO are shown in Figures 4.9 and 4.11. In PA6/HDPE 80/20 blends added with ZnO, the effect of addition of ZnO on the T_c peak of PA6 and HDPE components is relatively similar to that of the no added ZnO. This implied that the presence of ZnO in the blend does not affect the crystallization of each component.

Figure 4.12 shows DSC melting thermogram of PA6/HDPE blends without compatibilizer. Thermogram of the pure PA6 shows the two melting temperatures (T_m) at the shoulder peak 217.9°C and the sharp peak 220°C. These two melting temperatures have been reported that they represent the two kinds of crystal structure in polyamide, the melting temperature at 217.9°C corresponds to γ-form, and the melting temperature at 220°C corresponds to α-form. For the pure HDPE, the T_m peak occurs at 129.9 °C. The T_m peaks of each component in the PA6/HDPE blends are not difference from both neat polymers.

Melting thermograms of PA6/HDPE blends with compatibilizer are reported in Figures 4.13 and 4.15. The addition of compatibilizer resulting in lowering the T_m peak of both PA6 and HDPE components when compared with both pure polymers. For the PA6-rich blend (PA6/HDPE 80/20) (Figure 4.13), the presence of γ-form crystal can be correlated with the occurrence of interfacial interactions between polyamide and the compatibilizer phase. However, in the HDPE-rich blend (PA6/HDPE 20/80) (Figure 4.15), the γ-form melting temperature peak of PA6 was not observed. Melting thermograms of PA6/HDPE blends with compatibilizer and added ZnO are reported in Figures 4.14 and 4.16. The effect of added ZnO on the T_m peak of PA6 and HDPE components is relatively similar to that of no added ZnO.

For the weight fraction crystallinity (χ_c) of PA6 and HDPE components of PA6/HDPE blend with and without compatibilizer is presented in Tables 4.1. Fractional crystallinities for both PA6 and HDPE components in the blend is less than for the pure polymers, indicating that the crystallization of one component was affected by the addition of another component. However, the χ_c of PA6/HDPE blends with added ZnO is more than PA6/HDPE blends without ZnO.

Table 4.2 summaries the melting and crystallization temperatures of pure polymers and PA6/HDPE blends with and without compatibilizer, and with and without ZnO.

Mechanical properties

The tensile modulus of PA6/HDPE blends is shown in Figure 4.17. The tensile properties of compatibilized blends were studied to investigate the effect of Fusabond as a compatibilizer. An increase in the tensile modulus of PA6/HDPE blend was observed compared to the uncompatibilized blend. When a small amount of compatibilizer was added, the tensile modulus values of the compatibilized blend is gradually increasing. This behavior was unexpected, due to the fact that the crystallinity of the compatibilized materials was less. One possibility is that the distribution of crystallite size/spatial arrangement was different, leading to an increased tensile modulus.

The tensile strength of PA6/HDPE blends is shown in Figure 4.18. As expected, the tensile strength of the PA6/HDPE blends are enhanced by the addition of the compatibilizer. These values gradually increase as the amount of compatibilizer increased indicating that compatibilizer improved interfacial adhesion and caused the dispersed particle size to decrease, resulting in better stress transfer between two phases.

Elongation at break (%) of the PA6/HDPE blend is shown in Figure 4.19. Elongation at break of PA6/HDPE blends was also enhanced by the addition of the compatibilizer. The effect of compatibilization was more predominant in the PA6/HDPE 80/20 composition compared with the PA6/HDPE 20/80 composition. The addition of Fusabond® caused a percent elongation increase for the PA6/HDPE 80/20 from 22.8% to 263.8%. The increase in elongation suggests better stress transfer across the interfaces. The enhancement in mechanical properties suggests a strong interaction at the interface due to the presence of compatibilizer [12] and reduced stress concentrations around dispersed particles. Thus, higher homogeneity can be achieved with respect to uncompatibilized blends [7].

Stress at break of PA6/HDPE as a function of Fusabond contents are shown in Figure 4.20. These values increase when the amount of compatibilizer increases, indicating that compatibilizer improved the interfacial adhesion and caused the dispersed particle size to decrease resulting in better stress transfer between two phases.

Figure 4.21 shows impact strength of PA6/HDPE blends. The addition of compatibilizer in the PA6/HDPE blends caused a substantial increase in impact strength. This improvement can also be explained by the improved interfacial adhesion, which allows absorbed energy to transfer from one phase to another. The presence of the compatibilizer seems to ensure optimum stress transfer at the interface, thus enhancing the properties of these blends.

The Hardness of PA6/HDPE blends as a function of Fusabond® content is shown in Figure 4.22. The maximum improvement of hardness was observed when only 1.0 phr of Fusabond® was added to the PA6/HDPE blends.

In Figure 4.23 and 4.24 show the tensile strength of PA6/HDPE 80/20 and PA6/HDPE 20/80 blends with ZnO respectively. Adding ZnO to the polymer blend system does not increase the tensile strength vs. no added ZnO.

WAXS Analysis

WAXS patterns of melt-crystallized samples for neat PA6 and HDPE are presented in Figure 4.25, Pure PA6 gave pronounced two theta peaks at 20.45°C and 23.85°C associated with α_1-form(002) and α_2-form(200) crystal structure respectively. A characteristic peak at 21.4°C for the γ-form crystal structure was not observed [11]. Pure HDPE gave pronounced 2 theta peaks at 21.65°, 24.10°, 30.45° and 36.65° associated with (110), (200), (210) and (020) respectively. The crystal structure of (110) and (200) were ascribed to be orthorhombic crystal structures [13]. WAXS pattern of PA6/HDPE 80/20 is shown in Figure 4.26. Peak positions at similar angles were observed, indicating that the crystalline structure of the blend was not affected by the Fusabond content. WAXS pattern of PA6/HDPE blends with added ZnO is shown in Figure 4.27. The WAXS patterns were unaffected by the addition of ZnO. This result implies that ZnO did not affect the crystalline structure and is confirmed by WAXS patterns of PA6/HDPE 80/20 (Figure 4.28)

Dynamic Mechanical Analysis

Miscibility of polymer blends were studied using Dynamic Mechanical Analysis (DMA). DMA is often used to study polymer/polymer miscibility in polymer blends. The glass transition region can be studied using the loss modulus curves. The results of the dynamic mechanical testing thus add information to the behavior of the blends and the phase morphology. In this study the dynamic mechanical properties of blends were determined as a function of temperature dependence of storage modulus (E') and loss modulus (E"). The plot of loss modulus (E") as a function of temperature of pure component is shown in Figure 4.29. It was found that the PA6 exhibits two peaks at temperature of -79.9°C (β-relaxation), 37.7°C (α-relaxation) [12]. The γ-relaxation was not observed. The β transition, which is observed about -79.9°C, has been explained on the basis of the rotational

motion of water molecules [14] and/or the water polymer complex [15]. The α peak observed at about 37.7°C is ascribed to the glass transition temperature i.e. the onset of micro-Brownian motion of the chain segments [12]. These temperatures are in good agreement with reported data on PA6.

The peak of 46.9°C is a transition peak of HDPE which can be compared with those for polyethylene samples. In previous work, the DMA spectrum of polyethylene had three low-temperature peaks, at around -30 °C, -78 °C and -128 °C [9]; it is not clear what the molecular motion is that leads to these peaks.

From Figure 4.31 and 4.32 show the temperature dependence of loss modulus of PA6/HDPE blends with and without Fusabond. It was founded that T_g of compatibilized blend is less than T_g of uncompatibilized blend, peak shift from 35.4 °C to 31.3 °C and -79.1 °C to -72.9 °C. Figure 32 shows peak of the polymer blends at different Fusabond®. It was found that when the amount of Fusabond® increase T_g peak shift closer. This implied that the miscibility of polymer blend improve and also the result of the reduction of dispersed phase size was observed in the SEM results.

Figure 4.33 showed the DMA spectra of no added ZnO and added ZnO polymer blends at the composition PA6/HDPE 80/20 at 10 phr. of Fusabond®. It was found that there was a small shoulder at higher temperature, suggestive of a physical interaction between the inorganic phase and parts of the polymer matrix. The shift in E" to higher temperature in the chemically bonded system was larger, suggesting increased adhesion between the polymer blend system and the ZnO in this system [16]. However, when the amount of Fusabond® decrease (5 phr), there is no more difference between the added ZnO and no added ZnO in polymer blend system as shown in Figure 4.34, 4.35 and 4.36. This implied that the quantity of ZnO might be too small. This result is consistent with the results of SEM, mechanical properties and WAXS where there is no different found between added ZnO and no added ZnO.

4.5 CONCLUSIONS

HDPE-gMAH (Fusabond®) has been shown to be an effective compatibilizer for PA6/HDPE blends. SEM micrographs showed that the average size of the dispersed phase decreased significantly by the addition of small amount of Fusabond®. Only 1.0 wt% of Fusabond® was sufficient to produce maximum reduction in dispersed phase size. The decrease in crystallization temperatures, melting temperatures and crystallinity of each component in the blends as compared with pure PA6 and HDPE also supported that PA6/HDPE blends were improved by adding compatibilizer. The mechanical properties increased with the addition of compatibilizer, including tensile modulus, tensile strength, stress at break, elongation at break, impact strength and hardness. Adding ZnO to partially neutralize the acid groups did not improve phase morphology, thermal behavior and mechanical properties. WAXS patterns of compatibilized and uncompatibilized blends gave peak positions at similar angles indicating that the crystalline structure of the blend was not affected by the compatibilizer. DMA data supported that the improvement in the miscibility properties of blends containing Fusabond® and ZnO was observed.

For the further study, the author would like to suggest increase the quantity of ZnO, increase % neutralized of MAH or change the method to neutralize. Other neutralization method such as the solvent neutralization method may be worth considering in order to improve the efficiency of neutralize MAH by zinc cation. Moreover, using stearate acid to enhance the solubility of ZnO in the polymer matrix.

4.6 ACKNOWLEDGEMENTS

Authors are thankful to DuPont company (U.S.A.), TPE Co., Ltd., and UBE nylon (Thailand), for providing the materials for carrying out the present work.

4.7 REFERENCES

[1] Armet, R., and Moet, A., *Polymer*, 34(5), 977-985 (1993).

[2] Raval, H., Devi, S., Singh, Y.P., and Mehta, M.H., *Polymer*, 31(3), 493 (1991).

[3] Willis, J.M., and Favis, B.D., *Polym. Eng. Sci.*, 28, 1749-1757 (1993).

[4] Degée, Ph., Vankan, R., Teyssié, Ph., and Jerômé, R., *Polymer*, 38(15), 3861-3867 (1997).

[5] Valenza, A., Geuskens, G., and Spadaro, G., *Eur. Polym. J.*, 33(6), 957-962 (1997).

[6] Fairley, G., and Prud'homme, R.E., *Polym. Eng. Sci.*, 27(2), 1495-1503 (1987).

[7] Leewajanakul, P., Pattanaolarn, R., Ellis, J.W., Nithitanakul, M., Grady, B.P., J. *Appl. Polym. Sci.*, 89, 620-629 (2003).

[8] Macknight, W.J., and Lenz, R.W., *Polym. Eng. Sci.*, 25(18), 1124-1133 (1985).

[9] Sheng, J., Ma, H., Yuan, X.B., Yuan, X.Y., Shen, N.X., and Bian, D.C., *J. Appl. Polym. Sci.*, 76, 488-494 (2000)

[10] Willis, J.M., Favis, B.D., and Lavallee, C., *J. Mater. Sci.*, 28, 1749-1757 (1993).

[11] Lahor, A., Nithitanakul, M., Grady, B.P., *European Polymer Journal*. 40, 2409 (2004).

[12] Gadekar, R., Kulkarni, A., and Jog, J.P., *Journal of applied polymer science*, 69, 161 (1997).

[13] Psarski, M., Pracella, M., and Galeski, A., *Polymer*, 41(13), 4923 (2000).

[14] Mer, K. H., *Macromol. Chem.*, 38, 168 (1960).

[15] Curtis, A. J., *J. Res. Natl. Bur. Std.*, 65A, 185 (1961).

[16] Wu, C. S., *Journal of applied polymer science*, 92, 1749-1757 (2004).

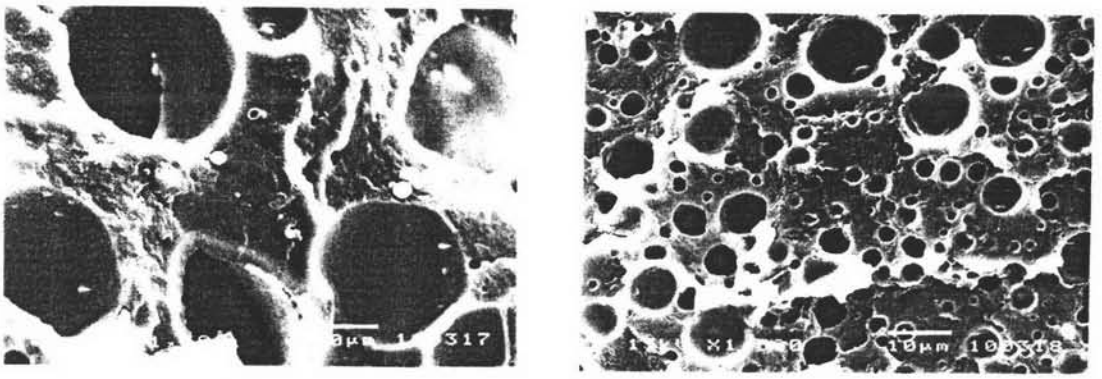

(a) (b)

Figure 4.1 SEM micrographs of blends without Fusabond® as a compatibilizer at the following PA6/HDPE ratios: (a) 80/20, (b) 20/80.

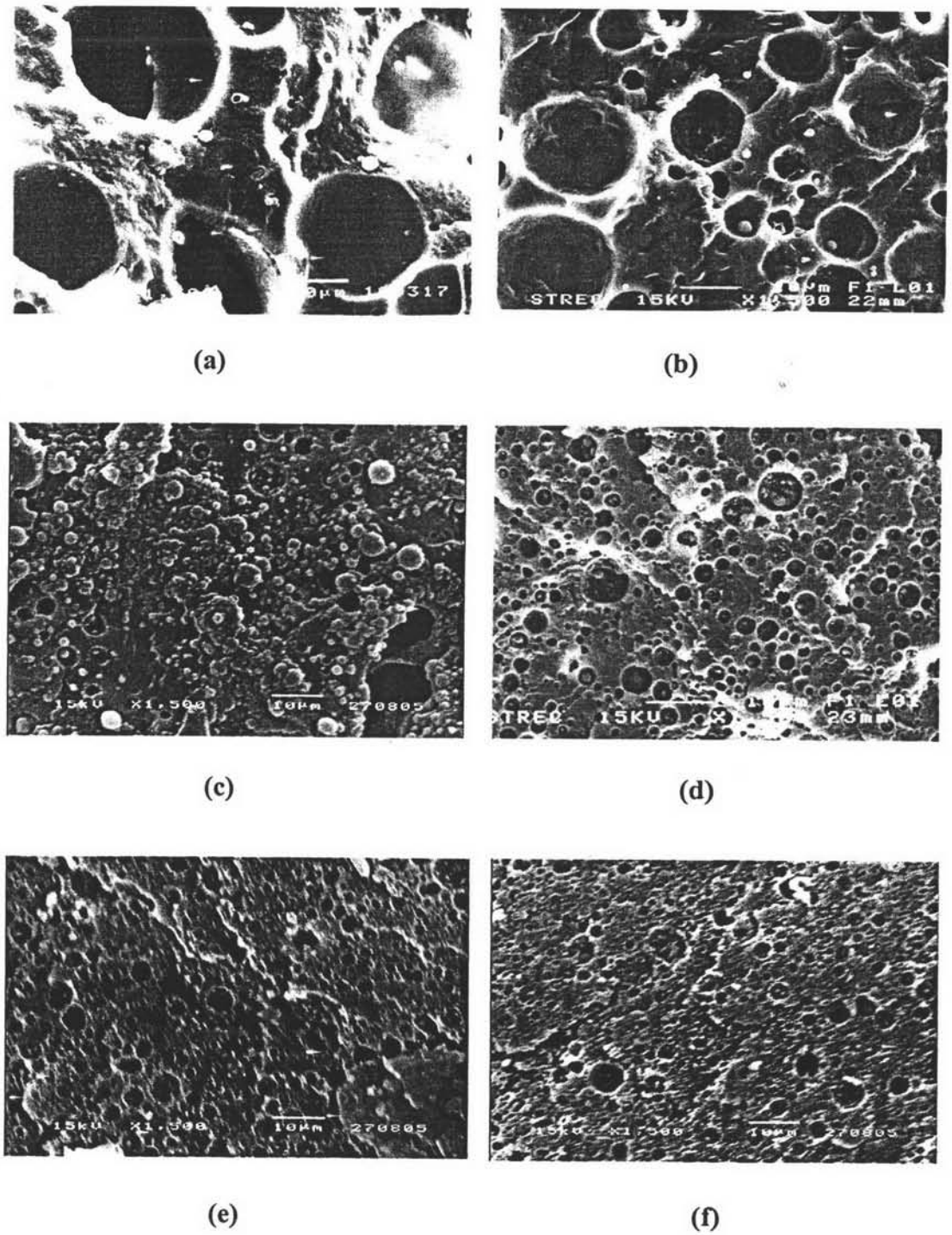

Figure 4.2 SEM micrographs of 80/20 PA6/HDPE blends with added Fusabond® compatibilizer at the following weight percentages: (a) 0, (b) 0.1, (c) 1.0, (d) 2.5 (e) 5.0 and (f) 10.0 phr.

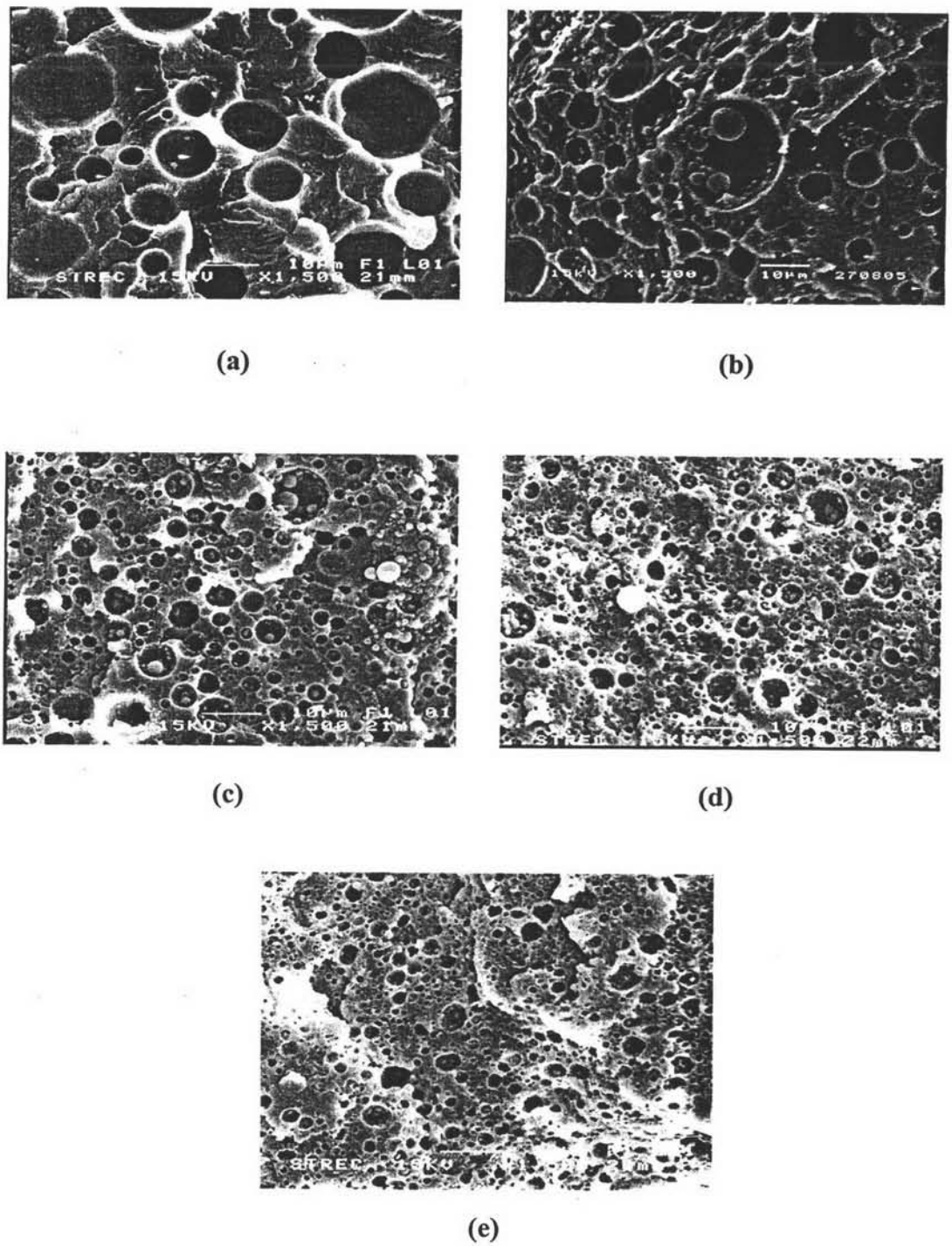

Figure 4.3 SEM micrographs of 80/20 PA6/HDPE blends with added Fusabond® compatibilizer at the following weight percentages: (a) 0.1 , (b) 1.0, (c) 2.5, (d) 5.0, and (e) 10.0 phr, with ZnO.

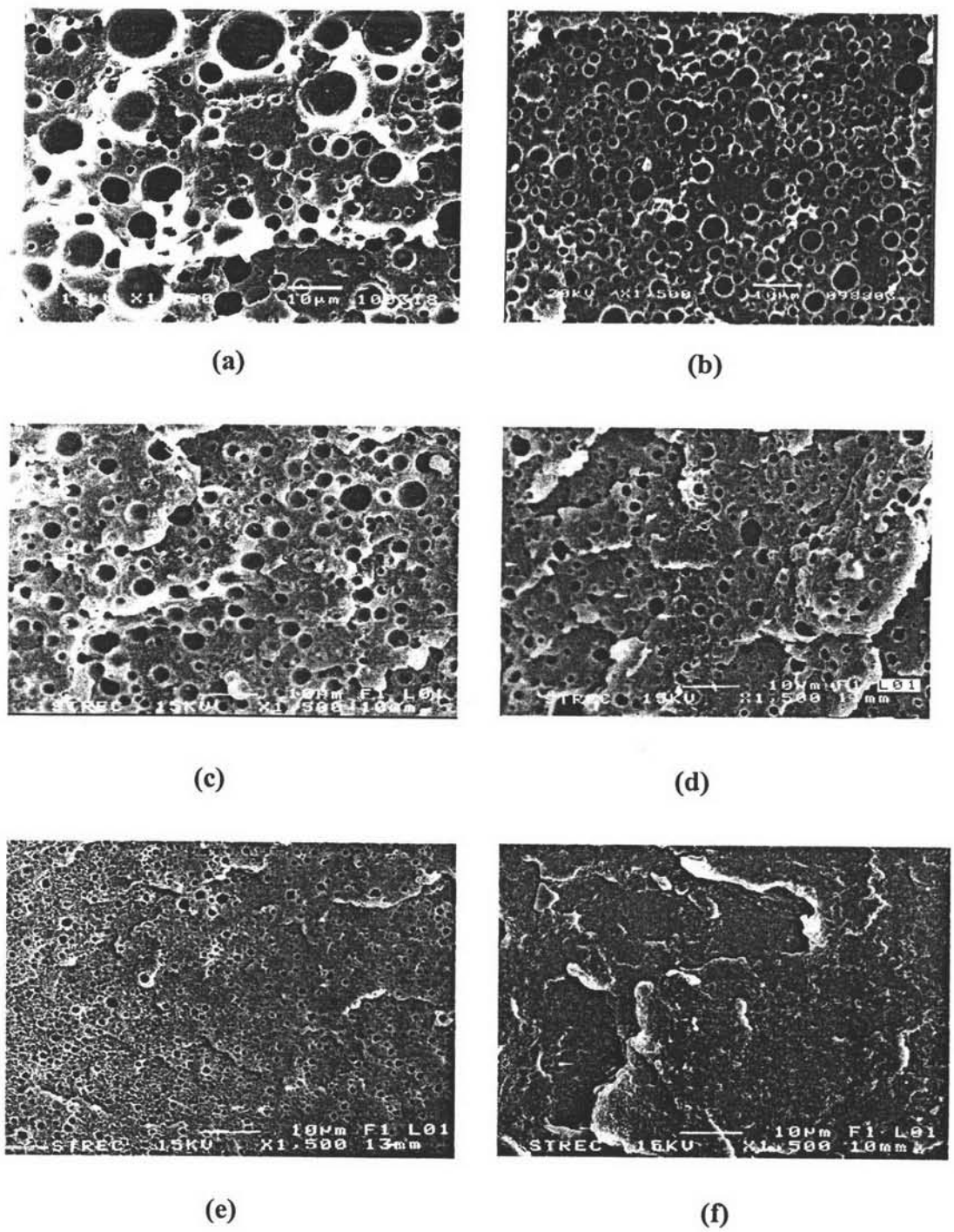

Figure 4.4 SEM micrographs of 20/80 PA6/HDPE blends with added Fusabond® compatibilizer at the following weight percentages: (a) 0, (b) 0.1, (c) 1.0, (d) 2.5, (e) 5.0 and (f) 10 phr.

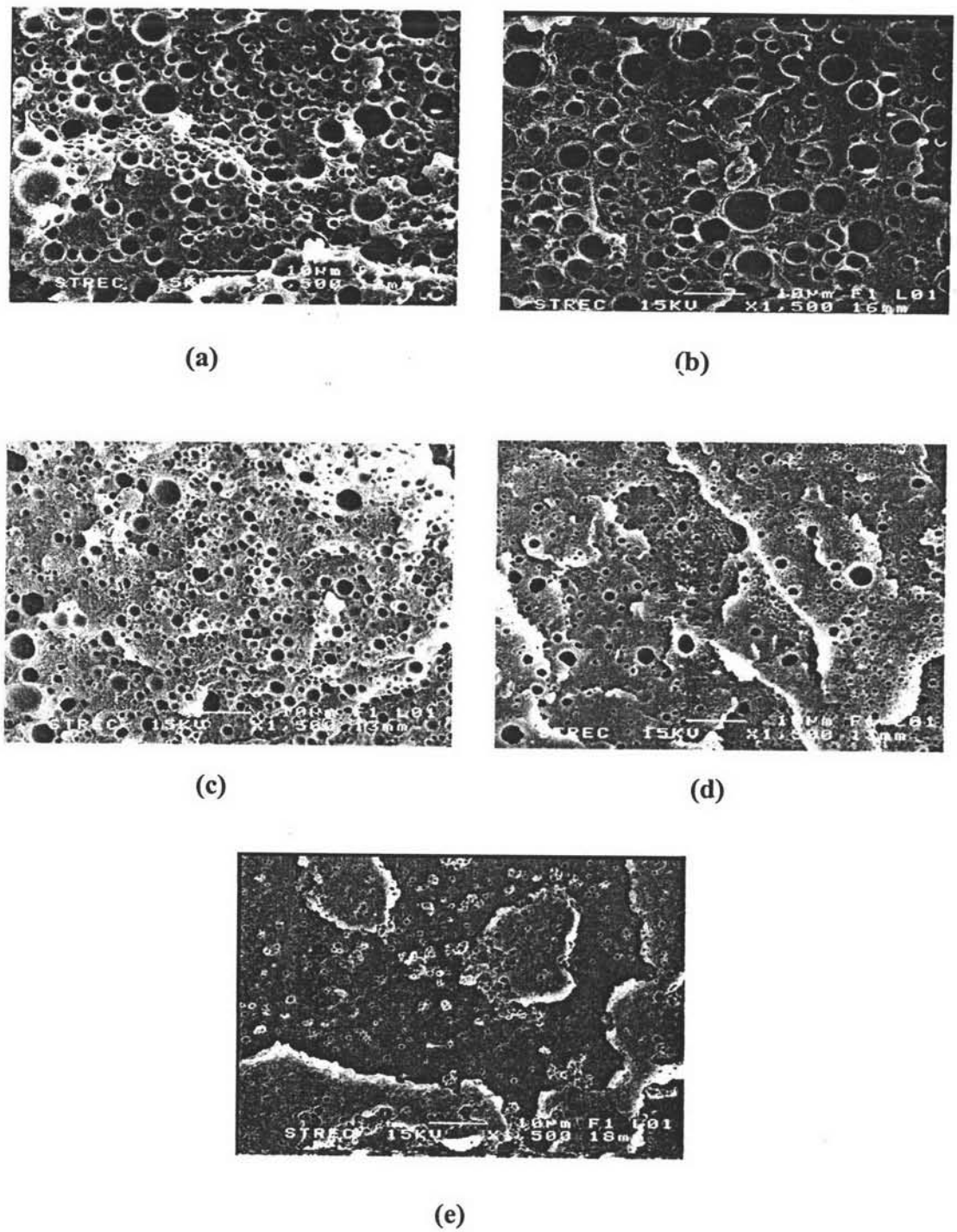

Figure 4.5 SEM micrographs of 20/80 PA6/HDPE blends with added Fusabond® compatibilizer at the following weight percentages: (a) 0.1, (b) 1.0, (c) 2.5, (d) 5.0, and (e) 10.0 phr, with ZnO.

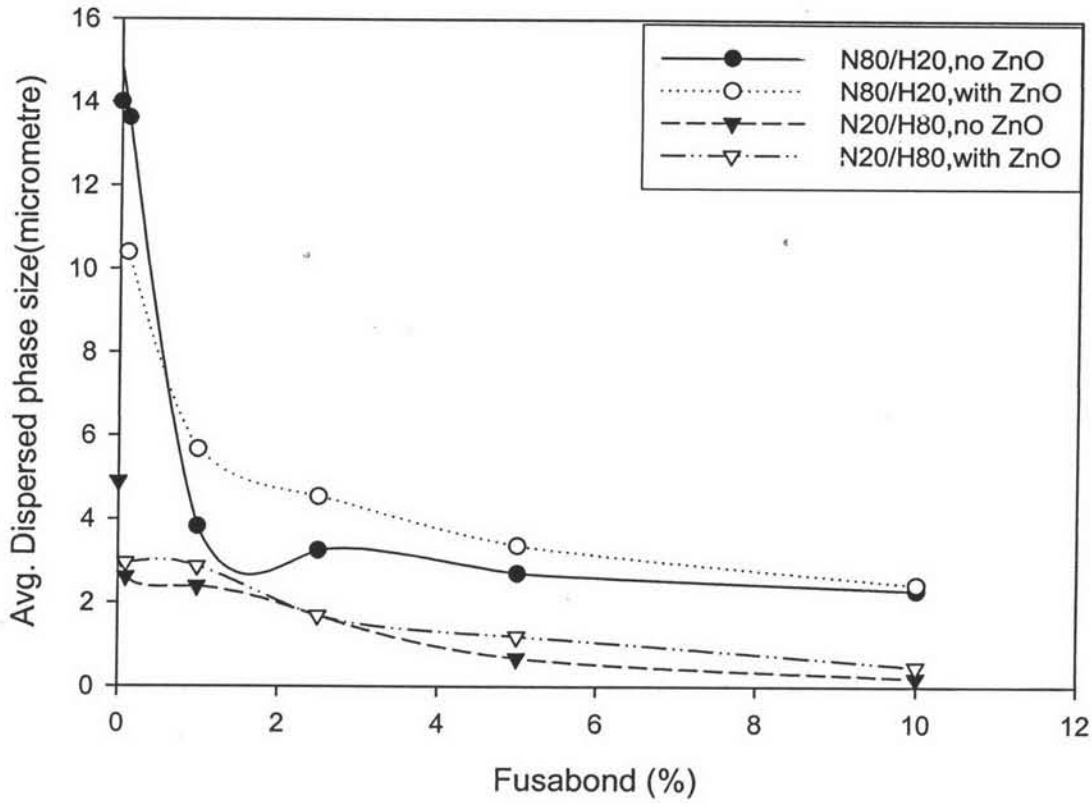

Figure 4.6 The dependence of the number average diameters measured as a function of Fusabond® content.

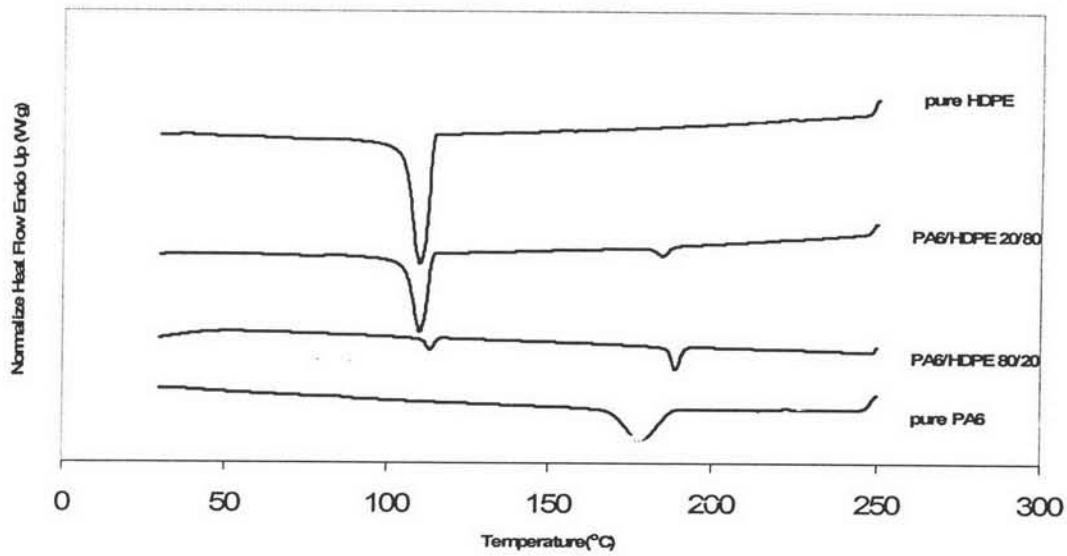

Figure 4.7 Crystallization temperatures of binary PA6/HDPE blends.

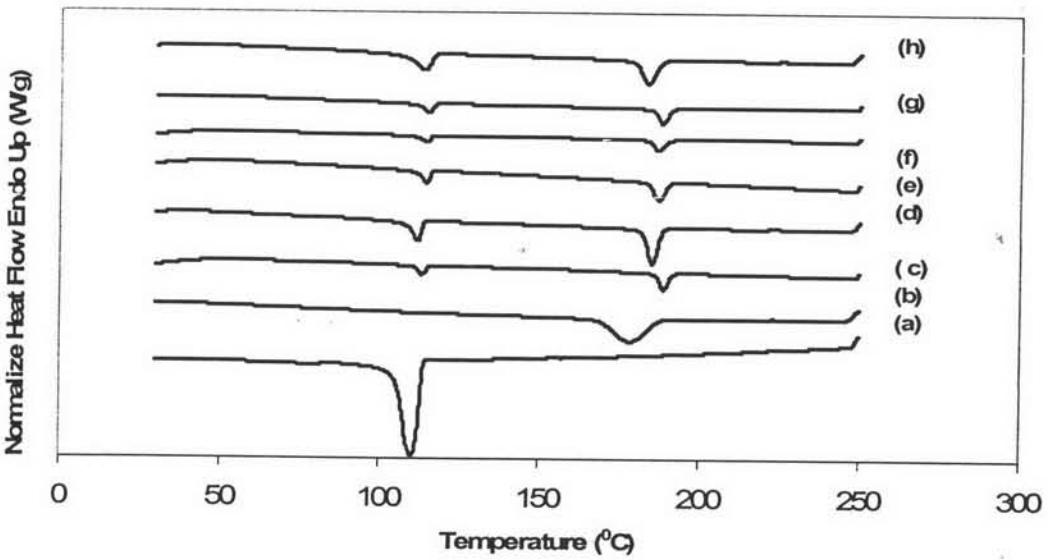

Figure 4.8 Crystallization temperatures of 80/20 PA6/HDPE blend as a function of Fusabond® content: (a) pure HDPE, (b) pure PA6, (c) 0%, (d) 0.1%, (e) 1%, (f) 2.5%, (g) 5%, (h) 10%.

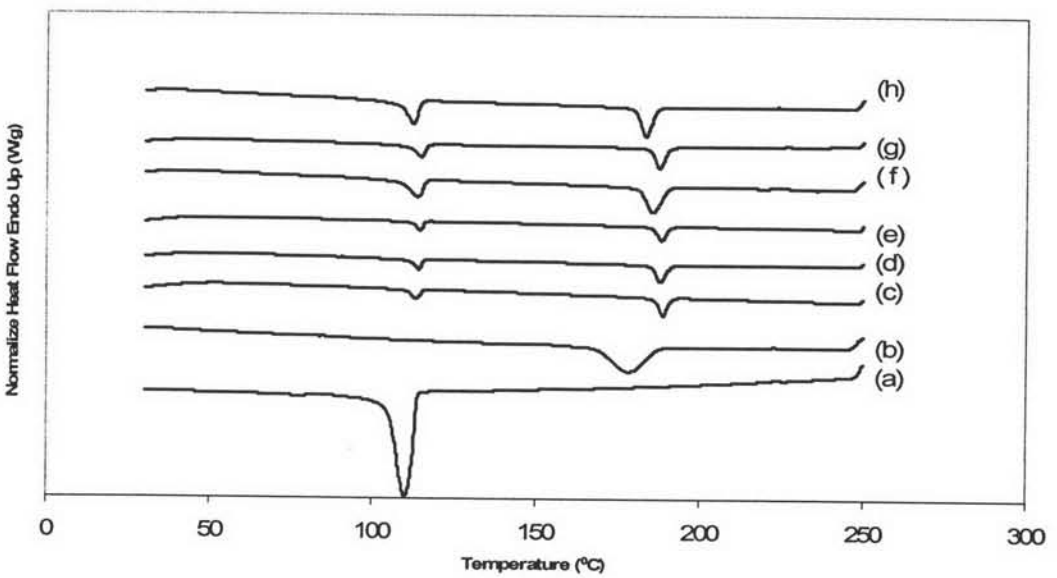

Figure 4.9 Crystallization temperatures of 80/20 PA6/HDPE blend as a function of Fusabond® content and ZnO: (a) pure HDPE, (b) pure PA6, (c) 0%, (d) 0.1%, (e) 1%, (f) 2.5%, (g) 5%, (h) 10%.

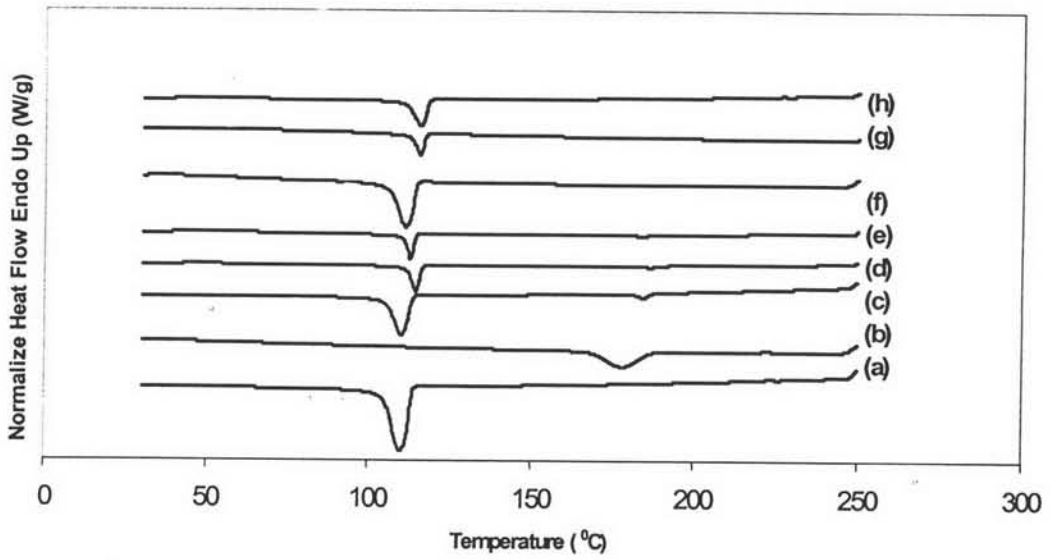

Figure 4.10 Crystallization temperatures of 20/80 PA6/HDPE blend as a function of Fusabond® content: (a) pure HDPE, (b) pure PA6, (c) 0%, (d) 0.1%, (e) 1%, (f) 2.5%, (g) 5%, (h) 10%.

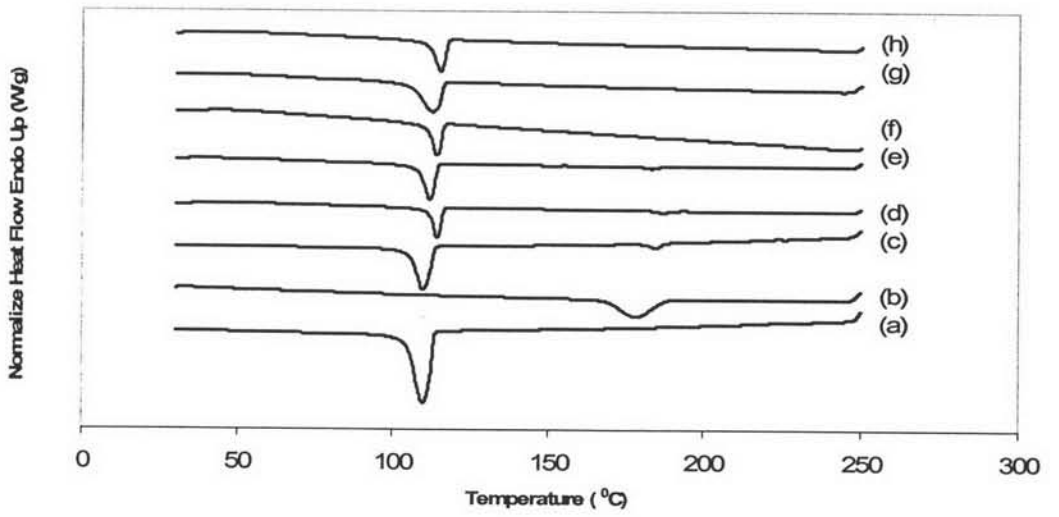

Figure 4.11 Crystallization temperatures of 20/80 PA6/HDPE blend as a function of Fusabond® content and ZnO: (a) pure HDPE, (b) pure PA6, (c) 0%, (d) 0.1%, (e) 1%, (f) 2.5%, (g) 5%, (h) 10%.

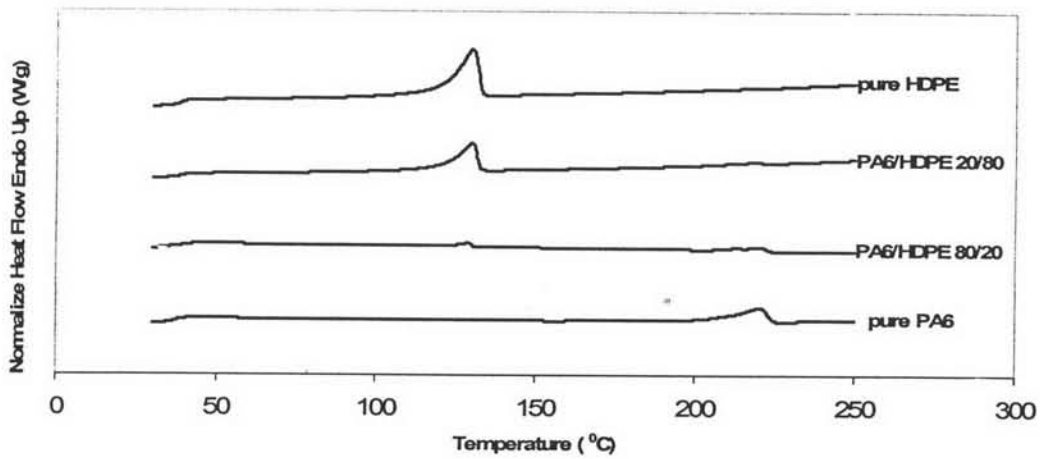

Figure 4.12 Melting temperatures of PA6/HDPE binary blends.

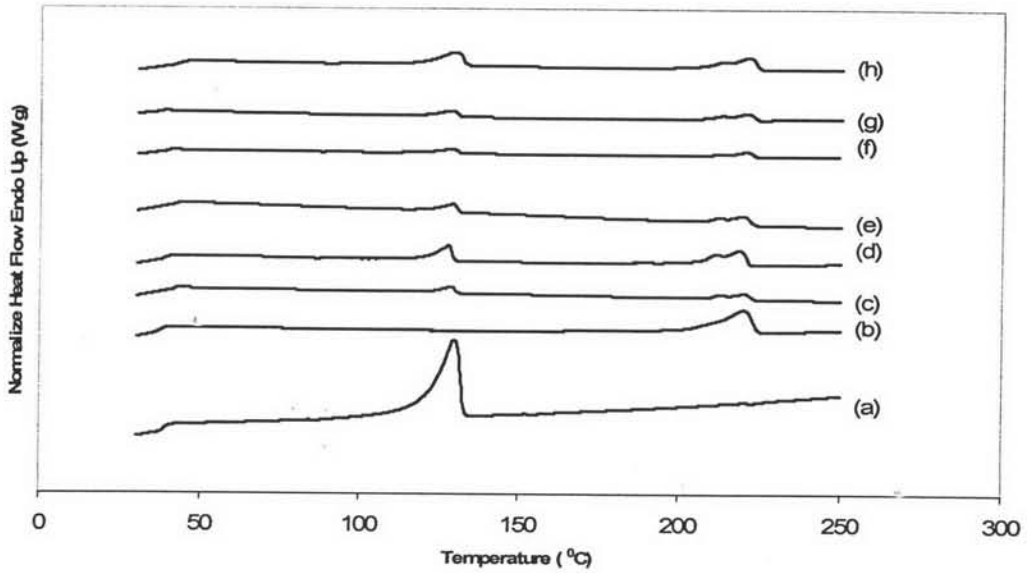

Figure 4.13 Melting temperatures of 80/20 PA6/HDPE blend as a function of Fusabond® content: (a) pure HDPE, (b) pure PA6, (c) 0%, (d) 0.1%, (e) 1%, (f) 2.5%, (g) 5%, (h) 10%.

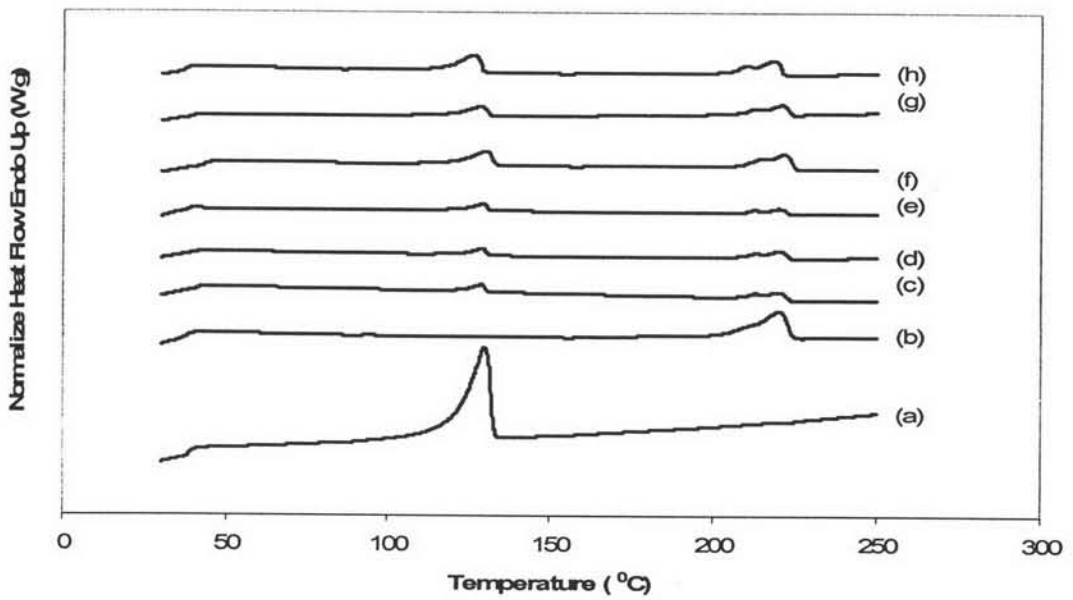

Figure 4.14 Melting temperatures of 80/20 PA6/HDPE blend as a function of Fusabond® content and ZnO: (a) pure HDPE, (b) pure PA6, (c) 0%, (d) 0.1%, (e) 1%, (f) 2.5%, (g) 5%, (h) 10%.

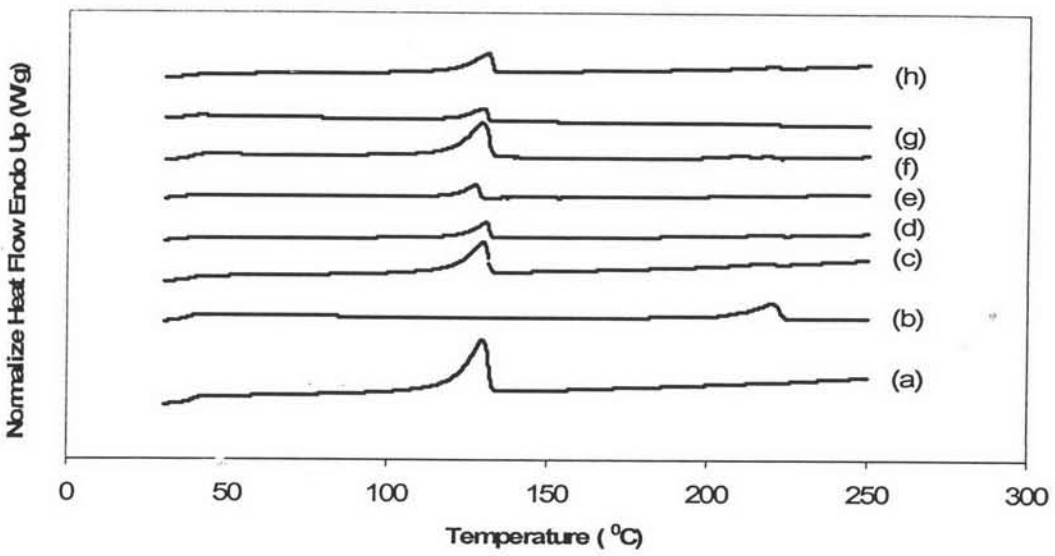

Figure 4.15 Melting temperatures of 20/80 PA6/HDPE blend as a function of Fusabond® content: (a) pure HDPE, (b) pure PA6, (c) 0%, (d) 0.1%, (e) 1%, (f) 2.5%, (g) 5%, (h) 10%.

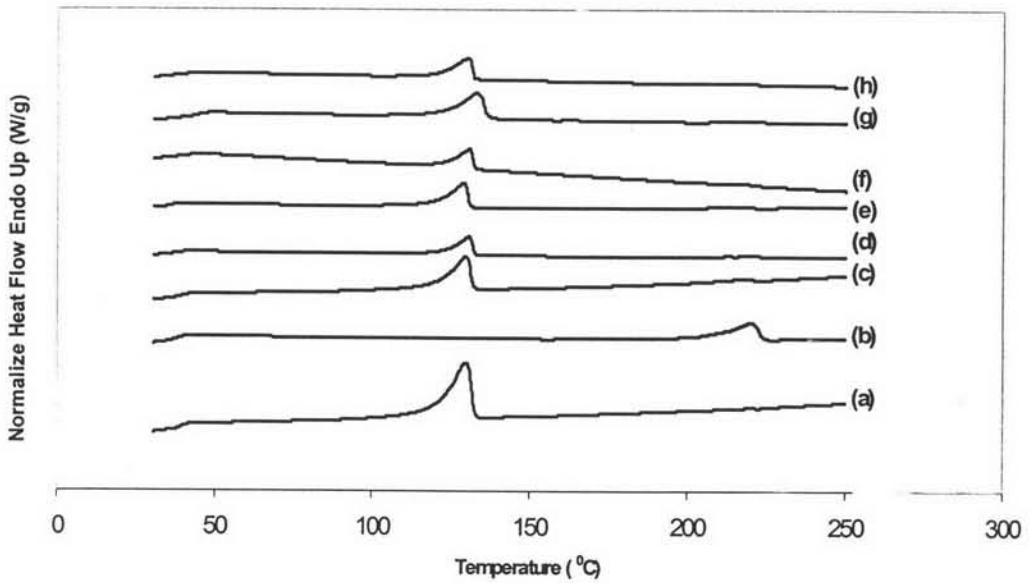

Figure 4.16 Melting temperatures of 20/80 PA6/HDPE blend as a function of Fusabond® content and ZnO: (a) pure HDPE, (b) pure PA6, (c) 0%, (d) 0.1%, (e) 1%, (f) 2.5%, (g) 5%, (h) 10%.

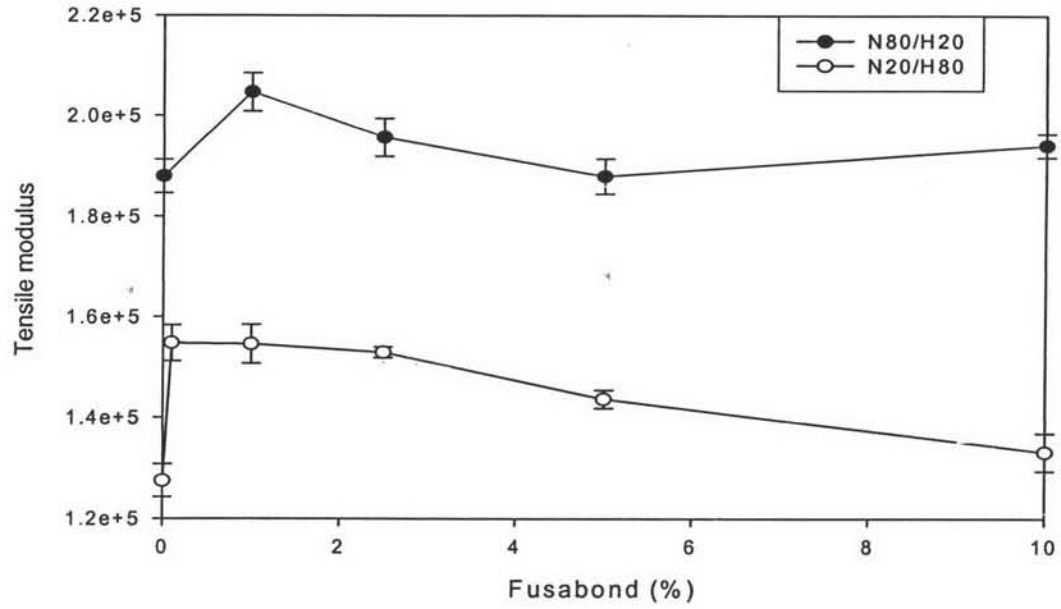

Figure 4.17 Tensile modulus (MPa) of PA6/HDPE blends as a function of Fusabond® content.

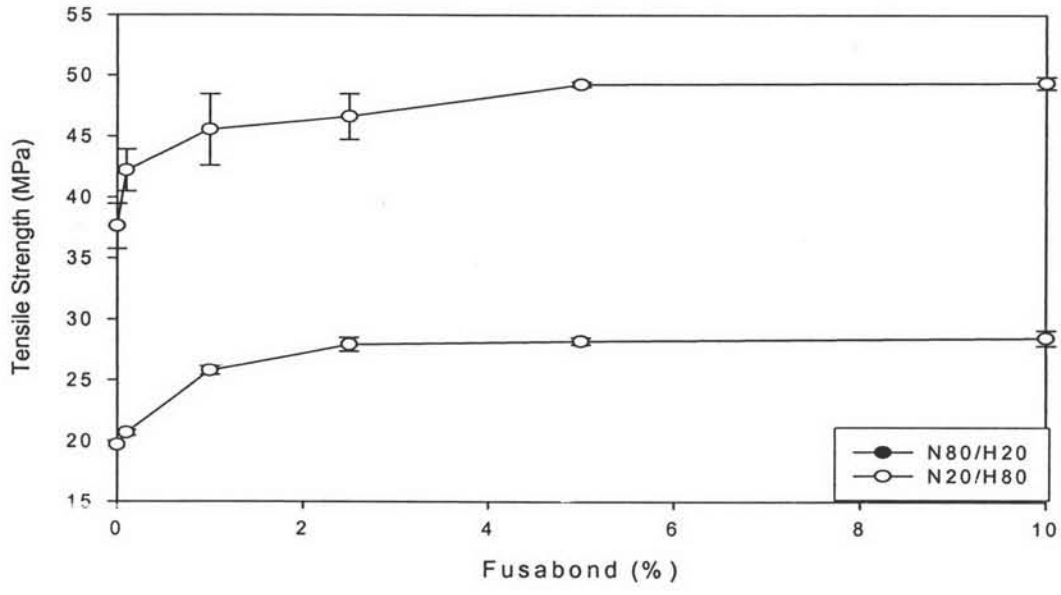

Figure 4.18 Tensile strength (MPa) of PA6/HDPE blends as a function of Fusabond® content.

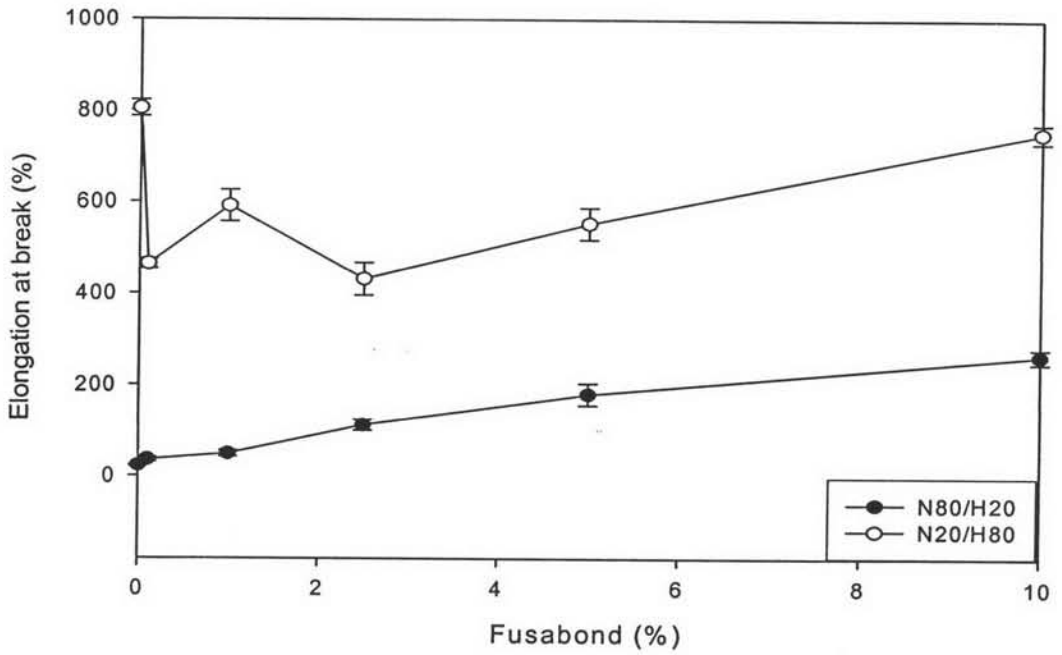

Figure 4.19 % Elongation at break of PA6/HDPE blends as a function of Fusabond® content.

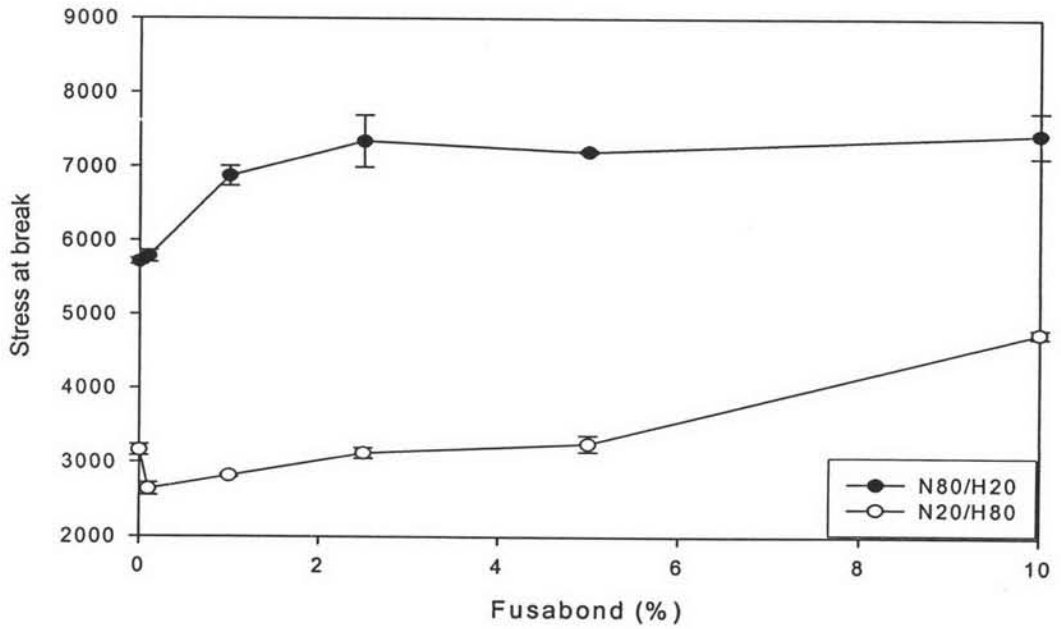

Figure 4.20 Stress at break (MPa) of PA6/HDPE blends as a function of Fusabond® content.

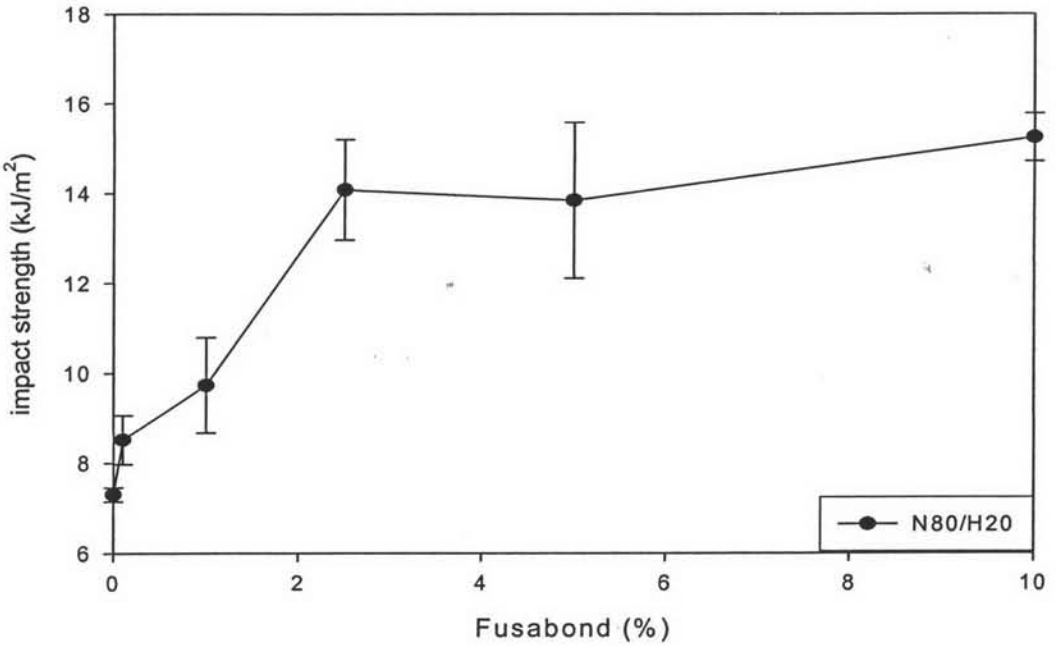

Figure 4.21 Impact strength of PA6/HDPE 80/20 blends as a function of Fusabond® content.

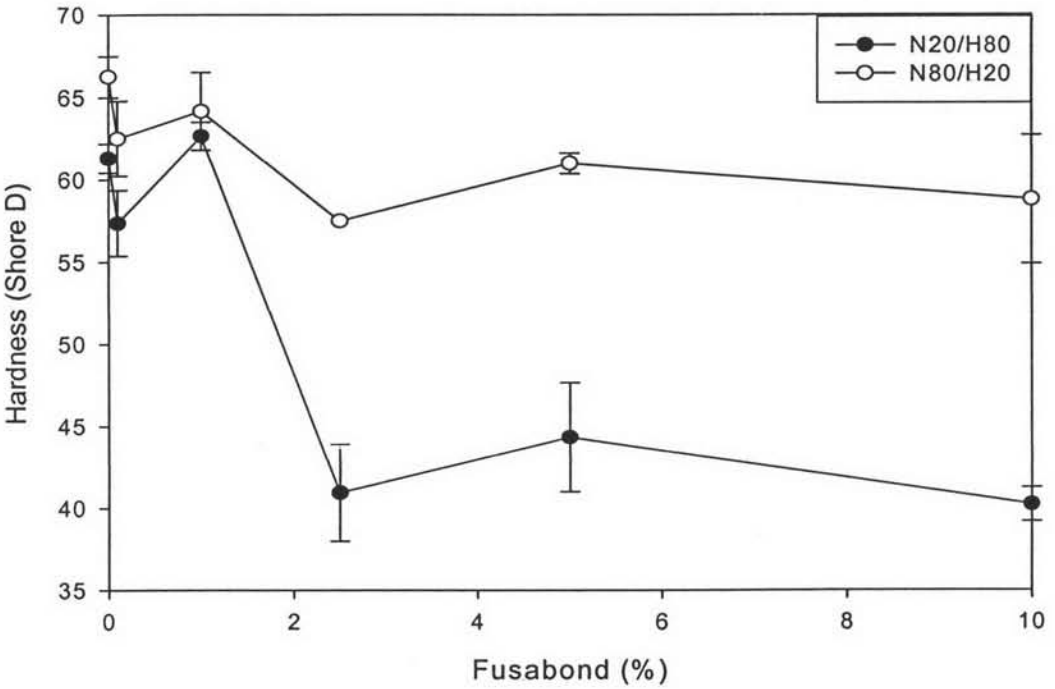

Figure 4.22 Hardness of PA6/HDPE blends as a function of Fusabond® content.

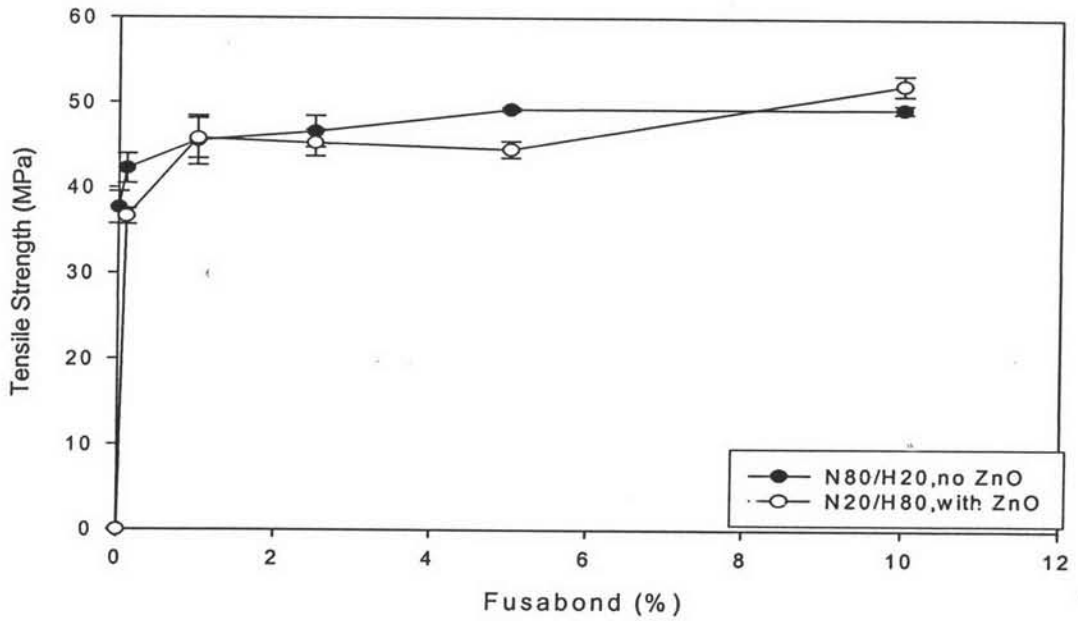

Figure 4.23 Tensile strength of PA6/HDPE 80/20 blends as a function of Fusabond® content.

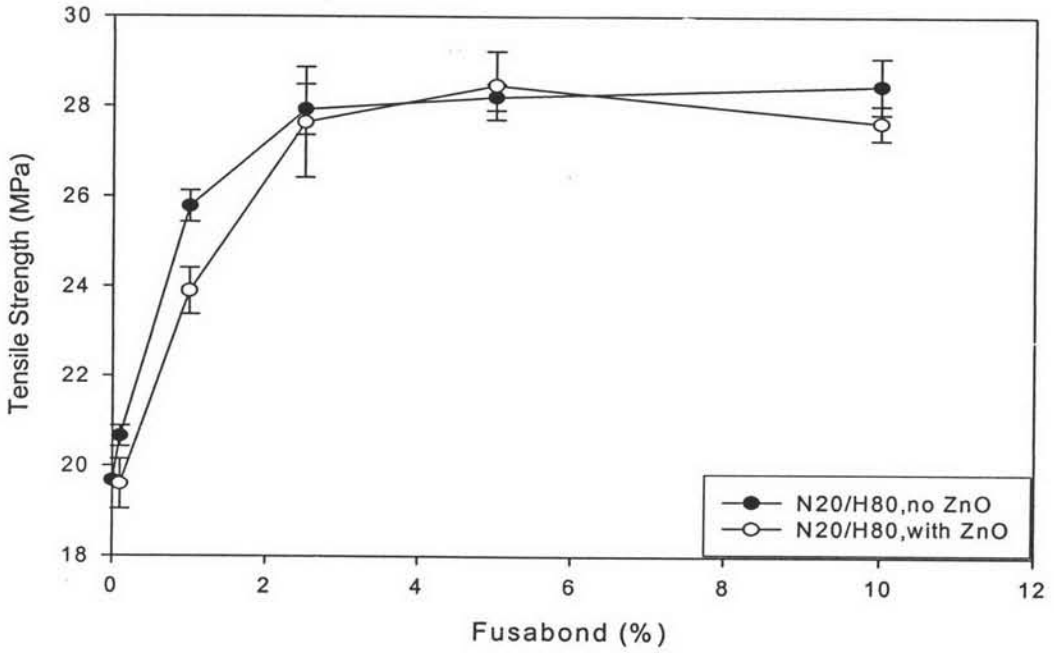

Figure 4.24 Tensile strength of PA6/HDPE 20/80 blends as a function of Fusabond® content.

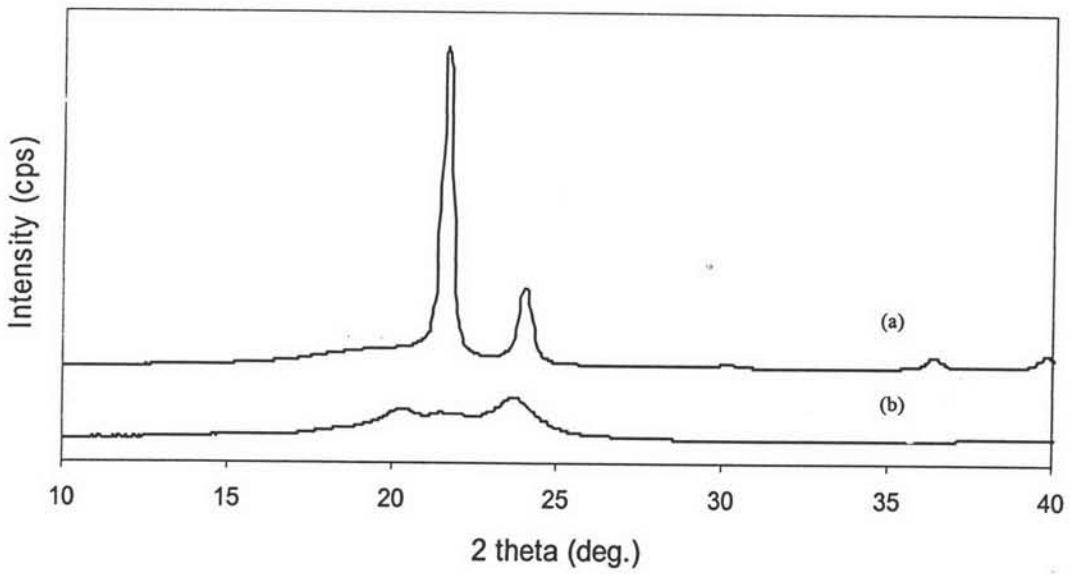

Figure 4.25 WAXS patterns of pure polymer: (a) HDPE and (b) Nylon6.

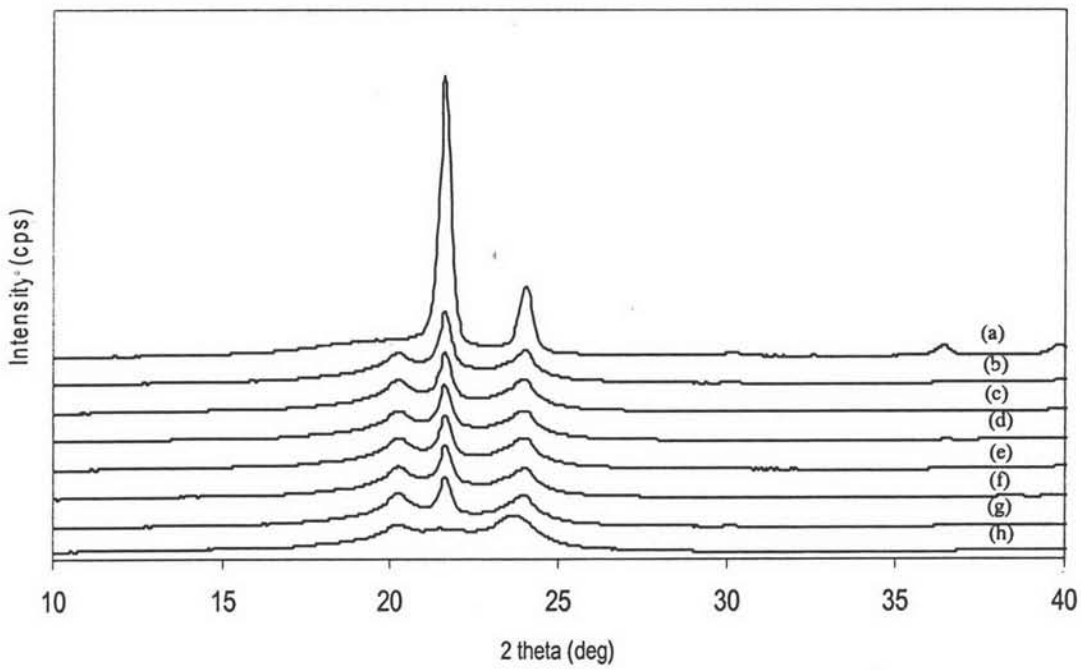

Figure 4.26 WAXS patterns of PA6/HDPE 80/20: (a) HDPE ,(b) 10 phr, (c) 5.0 phr, (d) 2.5 phr, (e) 1.0 phr, (f) 0.1 phr, (g) 0 phr and (h) Nylon6.

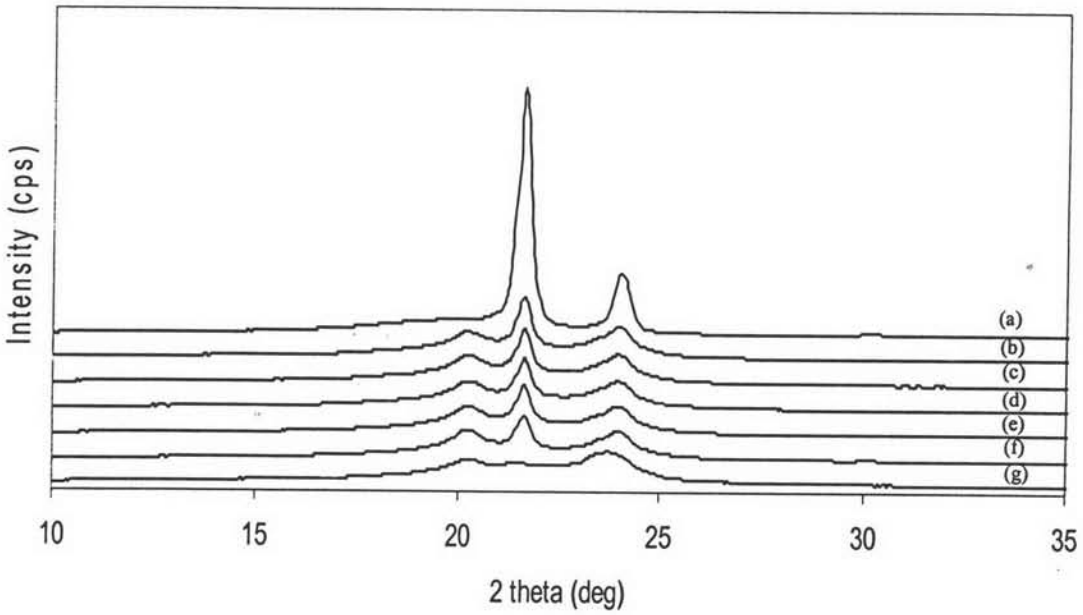

Figure 4.27 WAXS patterns of PA6/HDPE 80/20 with ZnO: (a) HDPE ,(b) 10 phr, (c) 5.0 phr, (d) 2.5 phr, (e) 1.0 phr, (f) 0 phr and (g) Nylon6.

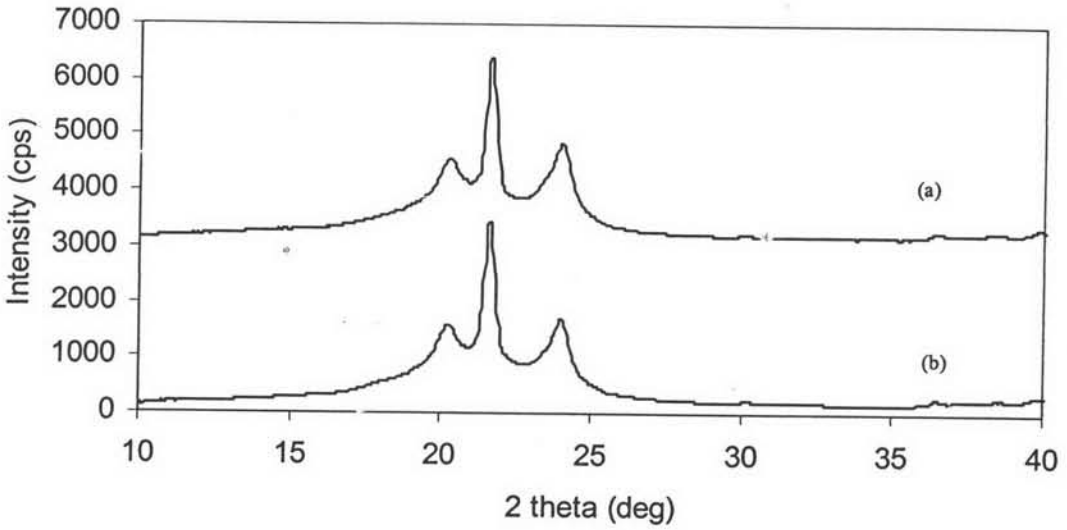

Figure 4.28 WAXS patterns of PA6/HDPE 80/20: (a) with ZnO and (b) no ZnO.

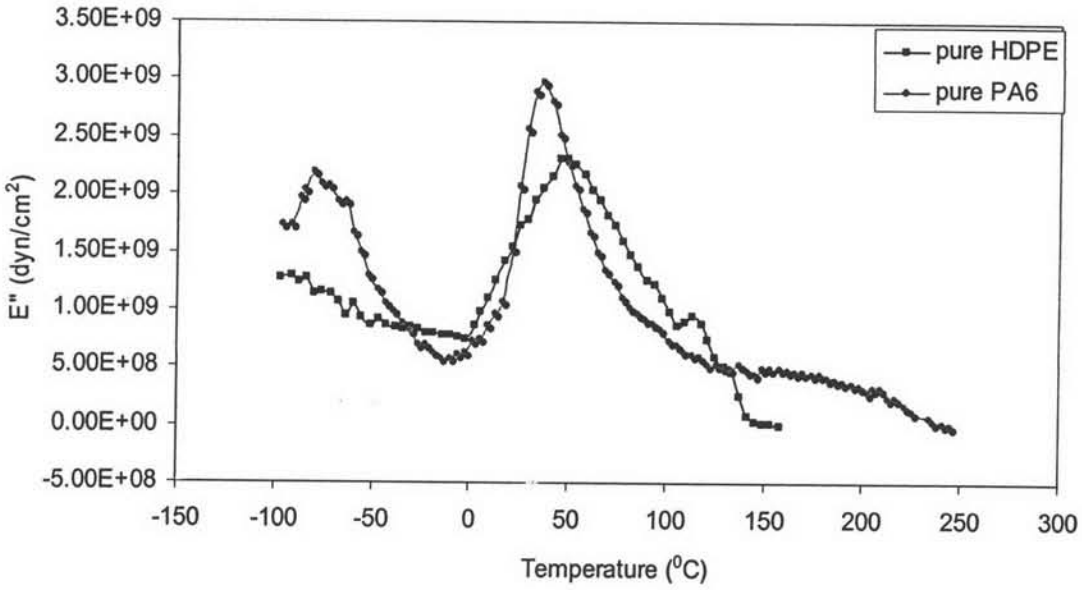

Figure 4.29 Temperature dependence of loss modulus of pure materials.

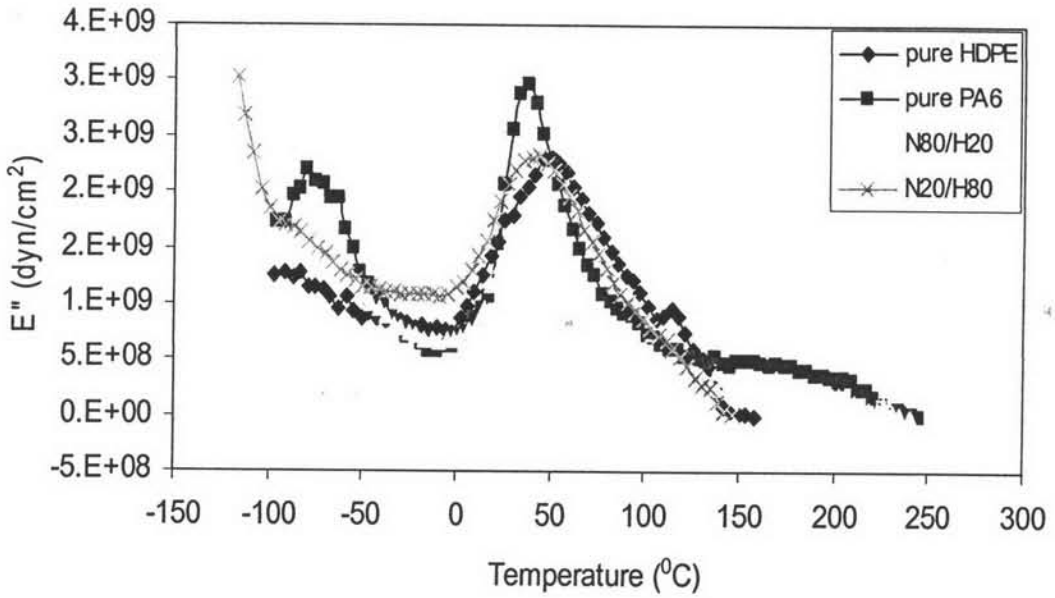

Figure 4.30 Temperature dependence of loss modulus of pure materials.

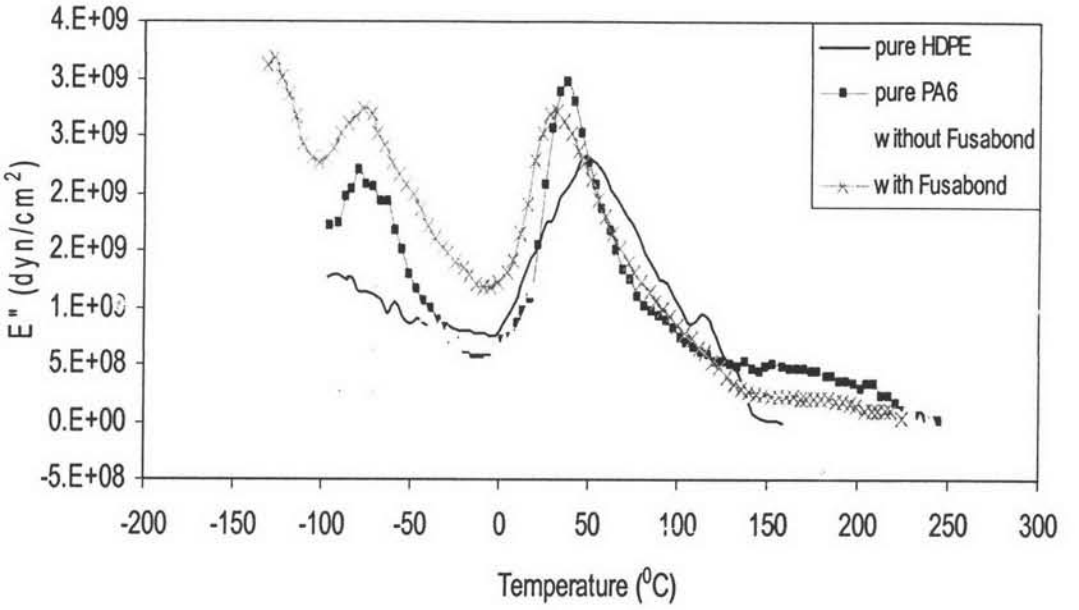

Figure 4.31 Temperature dependence of loss modulus of PA6/HDPE blends with and without compatibilizer.

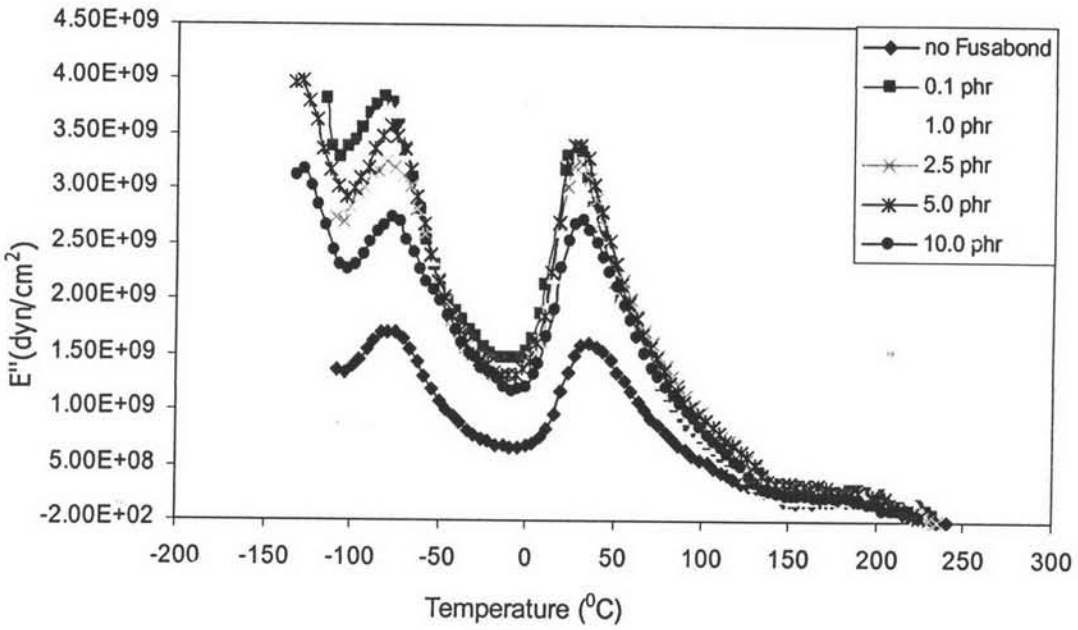

Figure 4.32 Temperature dependence of loss modulus of N80/H20 blends with and without compatibilizer.

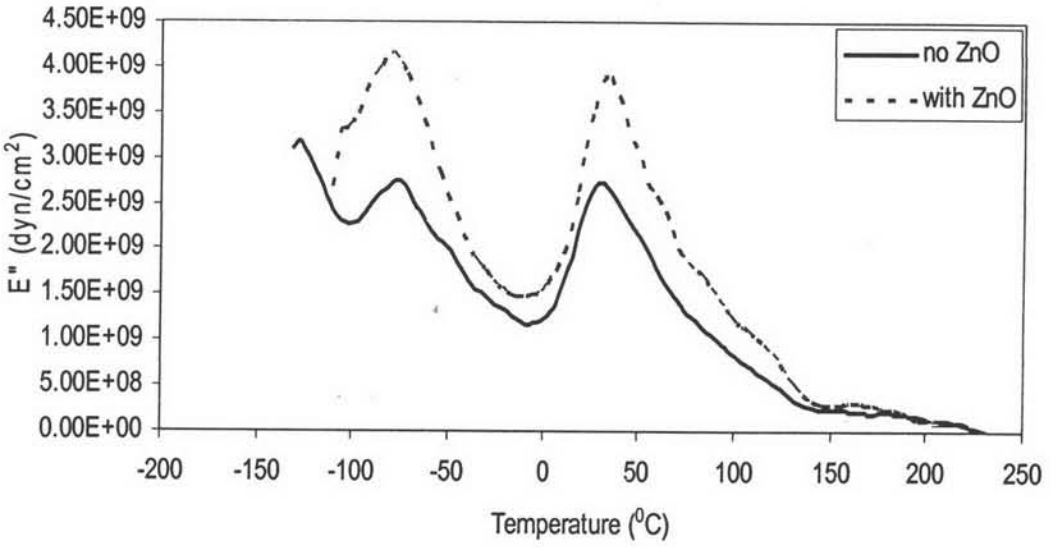

Figure 4.33 Temperature dependence of loss modulus of N80/H20 at 10 phr of Fusabond®.

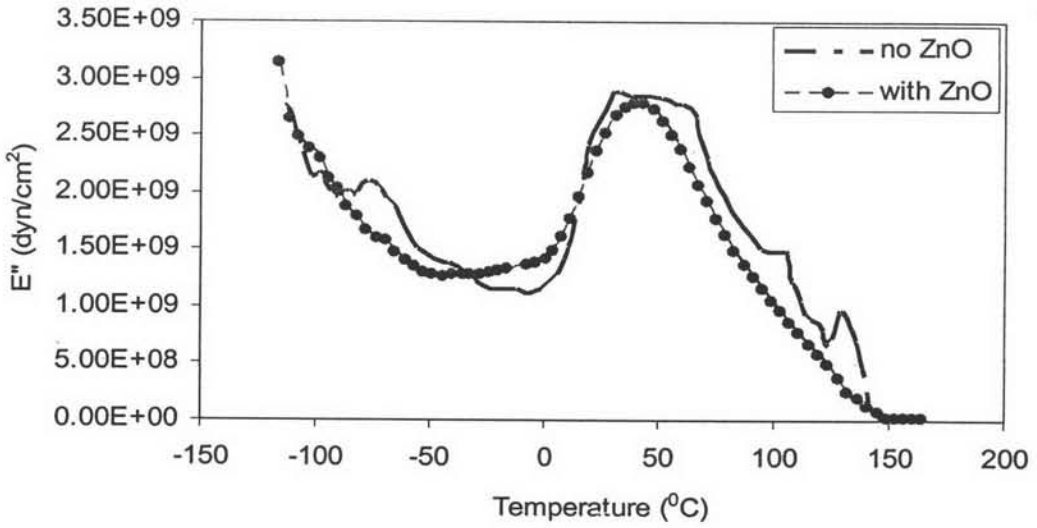

Figure 4.34 Temperature dependence of loss modulus of N20/H80 at 10 phr of Fusabond®.

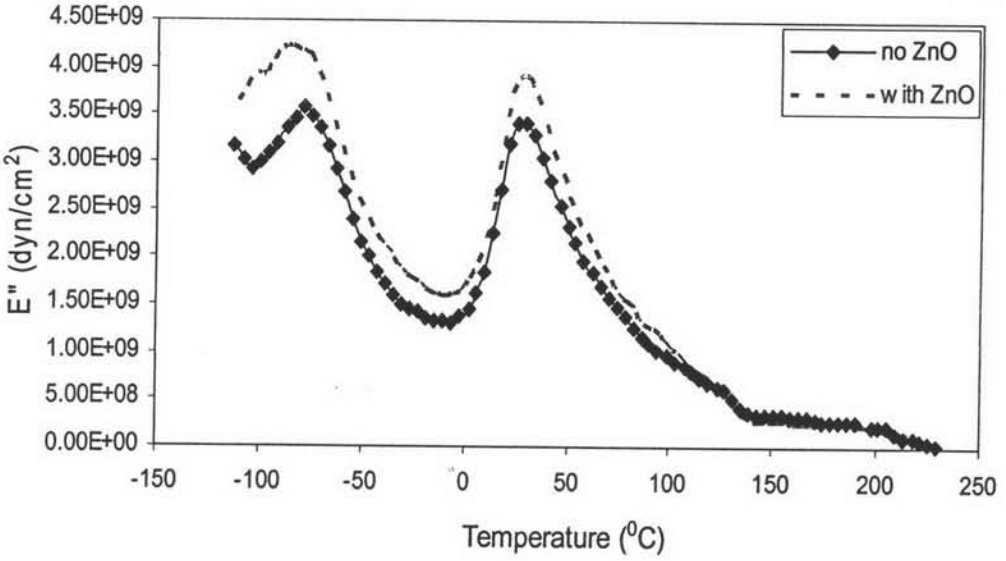

Figure 4.35 Temperature dependence of loss modulus of N80/H20 at 5 phr of Fusabond®.

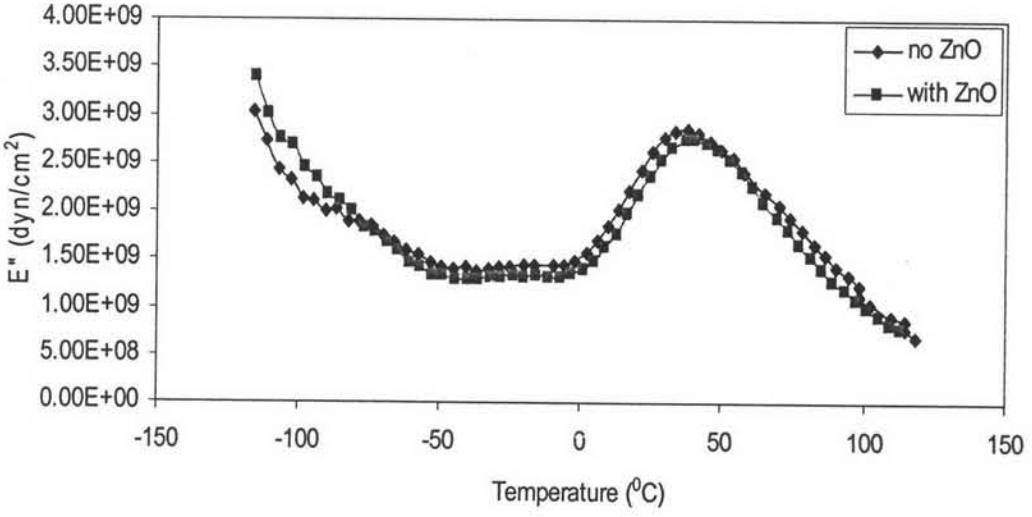

Figure 4.36 Temperature dependence of loss modulus of N20/H80 at 5 phr of Fusabond®.

Table 4.1 The weight fraction of crystallinity of PA6 and HDPE component in PA6/HDPE/HDPE-g-MAH (Fusabond®) ternary blends as determined by DSC

HDPE-g-MAH (Fusabond®) (%wt)	PA6/HDPE ratio			
	80/20		20/80	
	Crystallinity of PA6 (%)	Crystallinity of HDPE (%)	Crystallinity of PA6 (%)	Crystallinity of HDPE (%)
0	30.29	40.14	27.50	50.48
0.1	34.29	46.57	-	47.75
1.0	29.68	38.97	-	51.11
2.5	28.38	40.59	-	54.99
5.0	26.90	42.49	22.48	47.46
10.0	27.29	53.97	23.78	49.74
0.1/ZnO	30.98	33.15	22.62	47.73
1.0/ ZnO	29.50	39.98	19.47	50.25
2.5/ ZnO	31.89	52.15	-	47.92
5.0/ ZnO	27.29	47.77	-	48.65
10.0/ ZnO	29.64	61.77	-	49.42

Pure HDPE = 53.30%

Pure PA6 = 36.34%

Table 4.2 Melting and crystallization temperature of PA6 and HDPE components in PA6/HDPE blends with and without Fusabond®, and with and without ZnO as determined by DSC

Blend composition PA6/HDPE/ Fusabond®	PA6					HDPE			
	Endothermic			Exothermic		Endothermic		Exothermic	
	$T_{m(onset)}$ (°C)	T_m^{γ} (°C)	T_m^{α} (°C)	$T_{c(onset)}$ (°C)	T_c (°C)	$T_{m(onset)}$ (°C)	T_m (°C)	$T_{c(onset)}$ (°C)	T_c (°C)
100/0/0	209.0	220.2	-	187.4	178.5	-	-	-	-
0/100/0	-	-	-	-	-	121.0	129.9	113.8	110.1
80/20/0	208.8	213.5	220.2	191.4	188.8	123.1	129.0	115.6	113.1
80/20/0.1	206.3	211.8	218.7	188.2	185.0	120.9	127.9	113.7	111.7
80/20/1.0	206.9	214.0	219.7	190.5	187.3	122.1	129.4	116.4	114.3
80/20/2.5	208.5	212.5	220.7	190.8	187.5	129.0	121.4	116.8	114.8
80/20/5.0	213.2	212.8	221.0	190.9	188.1	119.9	128.5	117.0	115.0
80/20/10.0	206.2	213.0	221.2	187.6	183.6	120.5	129.7	116.9	113.6
80/20/0.1/ZnO	208.5	213.1	220.4	191.2	188.1	123.1	129.5	115.8	114.1
80/20/1.0/ ZnO	220.0	213.0	220.4	191.0	188.3	123.9	129.7	116.1	114.5
80/20/2.5/ ZnO	208.8	210.0	218.7	187.4	183.0	118.3	127.9	113.8	111.1
80/20/5.0/ ZnO	208.2	212.6	220.9	190.7	187.6	119.2	128.7	116.8	114.6
80/20/10.0/ ZnO	209.9	210.0	218.4	186.9	183.5	117.4	126.2	114.6	112.3
20/80/0	208.2	218.9	213.0	187.6	184.6	120.9	130.0	113.8	110.1
20/80/0.1	214.4	212.1	220.9	190.0	186.8	123.5	130.9	116.6	114.5
20/80/1.0	207.5	217.9	210.0	188.1	184.3	120.5	127.5	114.4	112.8
20/80/2.5	204.6	210.9	-	-	-	119.7	129.4	114.6	111.3
20/80/5.0	209.4	219.9	-	-	-	121.7	129.9	117.3	115.6
20/80/10.0	208.3	220.0	-	-	-	121.8	131.0	118.2	115.6
20/80/0.1/ ZnO	214.1	-	220.4	190.6	187.1	123.8	131.0	116.6	114.5
20/80/1.0/ ZnO	211.5	-	220.5	186.9	183.5	123.2	131.5	116.7	114.3
20/80/2.5/ ZnO	219.1	-	222.5	189.1	185.8	123.0	131.0	116.5	114.3
20/80/5.0/ ZnO	210.9	-	222.4	-	-	123.1	133.2	116.6	112.8
20/80/10.0/ ZnO	225.9	-	219.9	-	-	121.2	130.5	117.7	115.5